Summer 2023

Temperature-Dependent Diffusion in Block Copolymer Organogels

Ridwana Bashar
rb070@bucknell.edu

I, Ridwana Bashar, do grant permission for my thesis to be copied.

Temperature-Dependent Diffusion in Block Copolymer Organogels

by

Ridwana Bashar

A Thesis

Presented to the Faculty of

Bucknell University

In Partial Fulfillment of the Requirements for the Degree of

Master of Science in Chemical Engineering

Approved:

Adviser: Kenneth Mineart

Department Chairperson: Timothy Raymond

Engineering Thesis Committee Member: James Maneval

Engineering Thesis Committee Member: Bekele Gurmessa

7/11/2023

Date

Acknowledgement

I would like to express my deepest gratitude to Dr. Kenny Mineart for giving me the opportunity to be a part of his research group. I could not have undertaken the research work without the guidance of Dr. Mineart. I am also grateful to him for providing me with the opportunity to participate in conference meetings. I would like to thank my thesis committee members, Dr. James Maneval and Dr. Bekele Gurmessa, for their valuable perspectives and thoughtful feedback. A special thanks to Diane Hall for her assistance throughout my research work.

Table of Contents

List of Figures

List of Tables

Abstract

Organogels are often considered for transport-based applications such as transdermal drug delivery vehicles and gel actuators due to their unique properties. Recent consideration of styrenic block copolymer based organogels' application in transdermal drug delivery requires an extensive investigation of drug diffusion behavior through these gels to assess their applicability. Temperature is a major influencing parameter on diffusion. The goal of this research is to better understand the impact of temperature on diffusion in styrenic triblock copolymer organogels. To accomplish this goal, we focused on three specific objectives: (*i*) accurately measure the diffusivities of a solute – AOT reverse micelles – through organogels made with one of the three mineral oil solvents – Squalane, Hydrobrite 200 and Hydrobrite 380 – at different temperatures, (*ii*) establish a meaningful understanding of these data by interpreting them with preexisting models, and (*iii*) explore the possibility of composition-diffusion superposition in these materials. Gels for each oil solvent were formulated with five different copolymer concentrations, and Fourier Transform Infrared (FTIR) spectroscopy was used to track the diffusion of AOT reverse micelle through the gels. Diffusivity values are interpreted using two theoretical models – a general Arrhenius model and the detailed model developed by Petit *et al.* Ultimately, both of the models represent our data well and provide diffusion activation energy of the solute through gels. The diffusion activation energy is shown to increase with an increase in gel solvent viscosity. Lastly, we observe that diffusivity through gels composed of different solvents can be superimposed into a single master series at a specified reference composition using viscosity data. The master data set can be used to extend the temperature range over which diffusivity can be assessed in gels.

1. Introduction

Tunable physicochemical properties and the broad operating temperature window of block copolymer organogels make them attractive for transport-based applications[1]. One of the most impactful applications of these organogels is in the field of transdermal drug delivery[2]. Therefore, understanding the precise behavior of drug transport through organogels would immensely benefit the medical community. Several investigations have begun to build this understanding, but all of them have been conducted at either ambient or biological temperature and none specifically consider the role temperature plays. The aim of this thesis research is to investigate temperature-dependent diffusion in organogels made with triblock copolymer and mineral oil.

The capability of block copolymers to spontaneously self-assemble into nanoscale microstructures provides them with many desirable properties. Organogels based on styrenic block copolymers are good candidates for transdermal drug delivery since their transport and mechanical properties can be easily tuned through formulation changes. Polymer concentration, polymer molecular weight and gel nanostructure each play an important role in determining the diffusivity of a certain drug through polymer gels. Temperature plays an equally important role in controlling diffusivity. Hence, the investigation of temperature-dependent diffusion is crucial in understanding transport through these materials yet there is a significant gap in research regarding the dependence of diffusion on temperature in polymer gels. Moreover, the available data for effect of temperature on diffusion in organogels is nonexistent. In order to better understand controlled drug release from organogels, this thesis investigates the temperature-dependent diffusion of a model drug through block copolymer organogels.

The goal of this research is to understand the temperature-dependent transport through block copolymer organogels including gels composed of various copolymer concentrations and different mineral oil solvents. To achieve this goal, the present thesis addresses three objectives:

I.   Quantify the diffusivity of a solute through gels with different copolymer concentrations and solvent viscosity for a range of temperatures

II. Interpret temperature-dependent diffusivity values based on existing theoretical models

III. Explore the applicability of a composition-diffusion superposition model for interpreting diffusivity values

2. Background

2.1 Transdermal Drug Delivery

While most drugs are taken orally, some of them lack desired efficacy as their concentrations get significantly lowered before they reach systemic circulation[3]. Moreover, irregular and incomplete absorption of drug may occur which can have adverse effects. Injectable drugs can help in these cases but are not always preferred by the patient due to their invasive nature causing pain and the requirement of a trained executor. Transdermal drug delivery systems (TDDS) can solve these problems as they are convenient for the patient and help avoid first pass metabolism. TDDS transport drugs to dermal or epidermal tissue of skin and then the drug enters the bloodstream[4].

Depending on the properties of the drugs and their release rates, TDDS are usually designed in one of four ways – matrix, reservoir, drug in adhesive and multilaminate (Figure 2.1). The common components in all of these designs are a backing to protect the patch from external damage, drug, and a pressure sensitive adhesive (PSA) to adhere the patch to skin. (Note, the liner is removed before application to the skin.) In matrix-type TDDS, the drug resides in a matrix reservoir that is separate from the adhesive layer. Alternatively, reservoir-type TDDS hold the drug within a fluid-like reservoir and release is controlled by an additional membrane. The simplest TDDS is the drug in adhesive (DIA)-type wherein the PSA layer serves the purposes of skin adhesion, drug reservoir and controller of drug release[5]. The multilaminate-type is similar to the DIA having a membrane between two layers of drug loaded PSAs. Transdermal drug delivery through DIA patches is quite popular as these are thin, flexible and comfortable due to having only two layers.
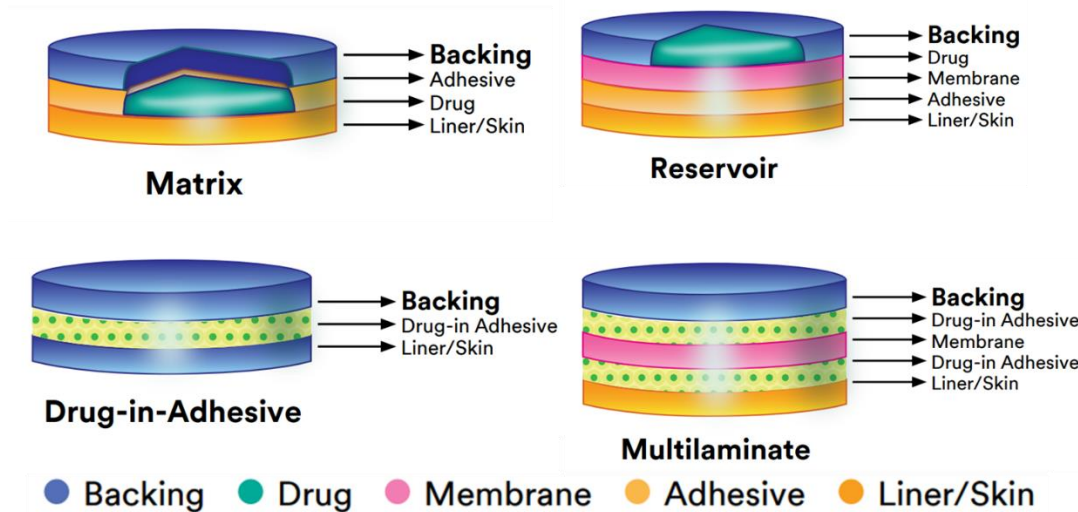
Figure 2.1: Types of transdermal drug delivery system designs. Image taken from Ref. 6

Styrenic block copolymers are commonly used to make PSAs in DIA patches[5]. Among

the styrene-based copolymers, styrene-isoprene-styrene (SIS) copolymer has been

researched as a PSA in transdermal patches. Ma *et* al.[5] were the first ones to use SIS in

PSA in a DIA patch. They made a testosterone-loaded transdermal patch and investigated

the drug loading capacity, the impact of the type and quantity of the permeation enhancer

on the patch's adhesive properties and skin permeation to optimize their formulation.

Their optimized formulation provided an in vitro drug release rate of 87.35 ± 5.78 µg/

$(cm^2. h^{1/2})$ as opposed to the release rate of 104.50 ± 9.67µg/ $(cm^2. h^{1/2})$ from

Testopatch® which is a commercial transdermal patch containing testosterone. To

investigate the in vivo pharmacokinetic behavior of the drug, the experimental and

commercial patches were applied to female rats separately. The plasma testosterone

concentration profiles over a 24-hour period for the experimental and the commercial

patches were found to be comparable. Their experiments showed that the experimental

patch had suitable constant skin permeation rate, good adhesion property and

pharmacokinetic parameters comparable to Testopatch® and assured that SIS is a feasible option to make the PSA component. In addition, a recent study[7] presented that transdermal patches made with styrene-(ethylene-co-butylene)-styrene (SEBS) copolymer demonstrated appropriate adhesive property and satisfactory biopharmaceutical properties. They used 9 wt% SEBS and ibuprofen as a model drug in their patch formulations. They observed that SEBS gels provided increased drug loading capacity up to 10 wt% as opposed to 3 wt%, which was achievable previously. This study further informed that drug release and skin permeation rate could be controlled by the molecular weight of SEBS. It was observed from a 24-hour in vitro permeation profile of ibuprofen that low molecular SEBS patches provide higher permeation than a commercial transdermal patch.

Even though styrenic block copolymers are being examined as drug delivery media, there is a research gap in the fundamental explanation for diffusion behavior of solutes through them. To overcome this gap, the Mineart Research group previously developed a method to determine diffusivity in styrenic block copolymer gels and investigated the impact of triblock copolymer concentration, block fraction and gel solvent on diffusivity of a solute[1,8–10]. Another study investigated transport of solute in organogels made with triblock copolymer/diblock copolymer/mineral oil[11].

2.2 Block copolymer self-assembly

One of the unique capabilities of block copolymers is their ability to self-assemble into various ordered nanoscale structures providing desirable transport and mechanical properties. By manipulation of appropriate parameters, several morphologies can be obtained. For simplicity and because of their similarity to triblock melt and gel phase

behavior, in this section, the phase behavior of diblock copolymer melts is presented in detail followed by the description of our intended gel system structure for the present research.

In a diblock copolymer (AB) melt, polymer pairs A and B are immiscible because of a positive heat of mixing and small entropy of mixing. Due to the unfavorable interaction between A and B, these two tend to separate from each other. But the separation of the blocks is limited as A and B are covalently bound and also because of loss of entropy caused by stretching the chains[12–14]. Microphase separation occurs through a balance of these two opposing phenomena and each block copolymer stays in separate phases forming ordered domains.

Degree of incompatibility, χN (χ is the Flory-Huggins segmental interaction parameter which is inversely proportional to temperature and N is the degree of polymerization), of a diblock copolymer melt represents the balance between the enthalpic contribution arising from the immiscibility of two distinct block copolymers and the entropic contribution arising from chain stretching. For a diblock copolymer melt the phase behavior depends on χN and copolymer composition, f_A,[15] where f_A is the volume fraction of block A. The value of f_A is responsible for the formation of interfacial curvature between the block copolymer domains and determines the type of ordered structure formed in the block copolymer melt. When χN is less than χN_{ODT} (ODT refers to order-disorder transition), a homogeneous disordered mixture of block copolymers will form (Figure 2.2 a). And as χN increases (Figure 2.2 a), and becomes greater than χN_{ODT}, different ordered morphologies, such as lamellar (L), gyroid (G, G'), cylindrical (C, C') or spherical (S, S') microdomains are observed[13].
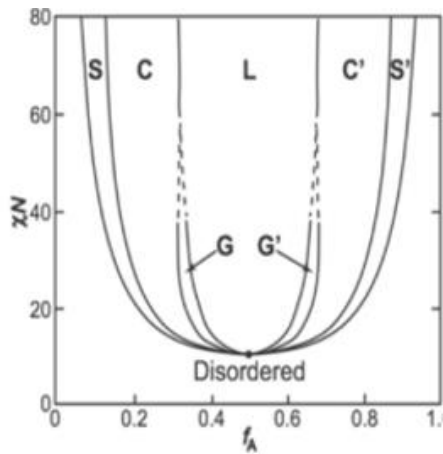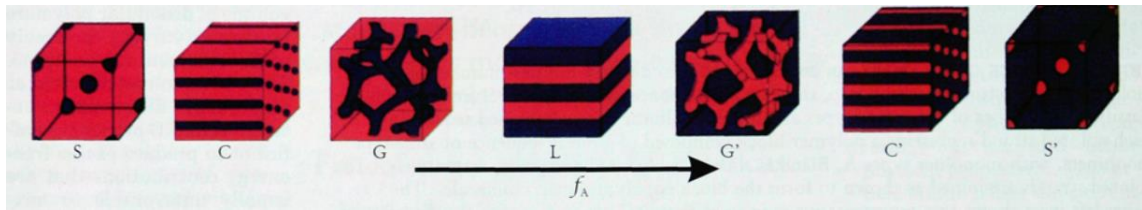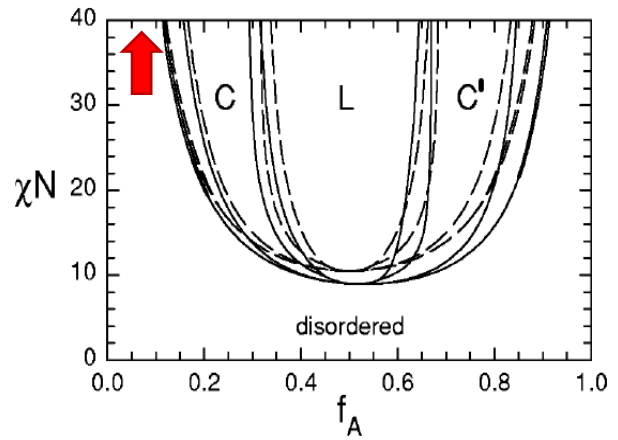
Figure 2.2: a) Theoretical phase diagram for AB diblock copolymers, b) AB diblock copolymer phase diagram (dashed curves) overlaid on the ABA triblock copolymer phase diagram (solid curves). The arrow indicates where the ABA gels made for this research approximately fall. Image taken from Refs. 16,17.

The phase diagram for a triblock copolymer (ABA) melt is similar to that of a diblock copolymer (AB) as the phase behavior of an ABA melt depends on the same factors as an AB diblock copolymer melt (Figure 2.2 b). However, there are some variations between their phase diagrams due the difference in their molecular architecture. In ABA triblock copolymer melts, the B midblocks stretch comparatively more than A endblocks causing domain asymmetry to be greater in case of ABA melts. Consequently, in the ABA triblock copolymer phase diagram, the phase regions move towards higher f_A, causing the phase diagram to become asymmetric (Figure 2.2 b)[17]. Introducing a solvent to a pure block copolymer melt to form gels would result

in a slightly different phase behavior since the interaction of blocks with the solvent would also need to be considered. Adding a block selective solvent has impacts on the copolymer χN as well as on the interfacial curvature of the microstructure formed[18]. In gels containing ABA triblock copolymer and a B block selective solvent, phase separation of A and B blocks may create several types of ordered phases. Though the driving force for the creation of these ordered morphologies is the degree of incompatibility between A and B block, concentration of the solvent and interaction between solvent and the blocks are also in control of determining the microstructure of gels[19]. Researchers have shown that the microdomain morphology of gels made with poly[styrene-(ethylene-*co*-propylene)-styrene] (SEPS) and a midblock selective solvent depends on the solvent fraction in gels as well as the compatibilities between midblock/solvent and midblock/endblock. These gels showed microdomain morphologies such as lamellae, cylinders and micelles as the polymer concentration in the gels was lowered[19]. Gel morphology plays a significant role in controlling diffusion. Therefore, investigation and selection of proper morphology is critical when designing a drug delivery medium. Gels made with a lower concentration of ABA triblock copolymer and a midblock selective solvent form spherical micelles in the disordered phase (see arrow in Figure 2.2 b) where these spherical domains are not organized in any order.[1,11] In these gels (Figure 2.3), A blocks are arranged in spherical domains devoid of solvent and the B blocks stay in the solvent. The ABA triblock copolymers either form loops, where B block coils back to the same micelle, or form bridges where spheres of A blocks are connected via B blocks[20]. Bridging is responsible for creating physical crosslinks in ABA gels.
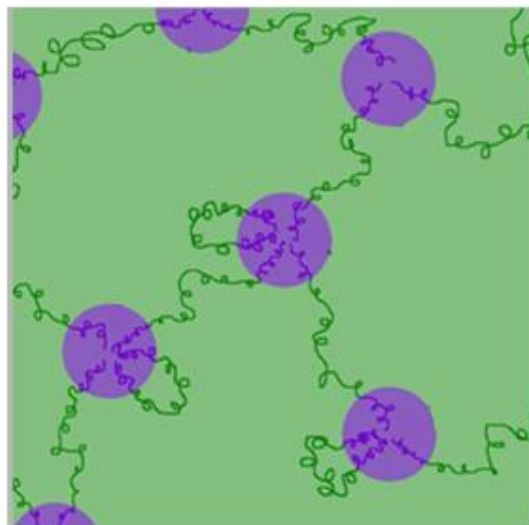
Figure 2.3: A cartoon depiction of a gel made with ABA triblock copolymer and a midblock selective solvent. A blocks (dark purple) are gathered in purple spheres and B blocks (dark green) are in the solvent (light green).

2.3 Diffusion in Block Copolymer Gels

Investigating the transport properties of drug molecules through block copolymer gels is one of the most important steps to determine their applicability in the pharmaceutical industry to ensure drug appropriate release time. To theoretically describe diffusion of a solute through gels, it is important to define the gel structure. As described in the previous section, the investigated gels form physically crosslinked networks that are swollen in solvent. This three-dimensional mesh-like structure contains glassy polystyrene domains and solvent filled regions where the midblocks reside. Diffusion occurs only through the solvent filled, midblock-containing regions. The distance between the midblock chains in the solvent filled regions can be characterized by 'mesh size'. Any factors such as increasing midblock concentration or reducing polymer chain mobility that reduces mesh size would reduce the diffusion through the gel[21]. The

diffusion properties of a polymer system are also significantly influenced by the size and shape of the diffusant and particular interactions within the polymer matrix[22]. It is found from literature that the bigger the diffusant the lower the diffusivity[23]. Temperature also plays an important role in controlling diffusion through gels[24] as diffusivity increases with the increase in thermal energy. Similarly, the viscosity of the gel solvent has a significant impact on transport through the gels as increased viscosity of solvents would reduce transport of the solute[10].

2.4 A Mathematical Model for Diffusion through gels

A mathematical model that will give us the diffusivity of a solute in the gels considered in this thesis is developed below. This is a macroscopic model that allows us to determine diffusivity from experiments based on their actual conditions.

Following the species equation of continuity, the differential mass balance for transport of species α through species β can be written as,

$$\frac{\partial \rho_\alpha}{\partial t} + \nabla \cdot (\rho_\alpha \boldsymbol{v}) + \nabla \cdot \boldsymbol{j_\alpha} = r_\alpha \qquad (2.1)$$

where ρ_α is the mass density of α, $\boldsymbol{v}$ is the mass velocity vector, $\boldsymbol{j_\alpha}$ is the molecular mass flux vector of species α, and r_α is a reaction rate expression with respect to α.

The mass flux, j_A, of species A according to the Fick's law of diffusion is,

$$j_\alpha = -\rho_t \, D_\alpha \nabla \, w_\alpha \qquad (2.2)$$

where ρ_t is the total mass density, w_α is mass fraction ($w_\alpha = \rho_\alpha / \rho_t$), and D_α is the diffusivity of solute α through β. Assuming constant total mass density, Equation (2.2) yields,

$$j_\alpha = -D_\alpha \nabla \rho_\alpha \tag{2.3}$$

Putting j_α from Equation (2.3) into the overall Equation (2.1) we find,

$$\left[\frac{\partial \rho_\alpha}{\partial t} + \nabla \cdot (\rho_\alpha \mathbf{v})\right] = -D_\alpha \nabla^2 \rho_\alpha + r_\alpha \tag{2.4}$$

Now, expressing Equation (2.4) in the cylindrical coordinate,

$$\left(\frac{\partial \rho_\alpha}{\partial t} + v_r \frac{\partial \rho_\alpha}{\partial r} + \frac{v_\theta}{r}\frac{\partial \rho_\alpha}{\partial \theta} + v_z \frac{\partial \rho_\alpha}{\partial z}\right) = -D_\alpha \left(\frac{1}{r}\frac{\partial}{\partial r}\left(r \frac{\partial \rho_\alpha}{\partial r}\right) + \frac{1}{r^2}\frac{\partial^2 \rho_\alpha}{\partial \theta^2} + \frac{\partial^2 \rho_\alpha}{\partial z^2}\right) + r_\alpha$$

$$\tag{2.5}$$

In the actual diffusion experiment a gel disk (β) loaded with species α is placed in a large

bath with excess solvent (the solvent is the same one used for gel formulation). The bath

is continuously agitated. The following assumptions can be made for our experimental

condition – no rate of production or degradation of α via reactions ($r_\alpha = 0$), no

convective mass transport (v_r, v_θ and $v_z = 0$); and no diffusion in the θ direction ($\frac{\partial^2 \rho_\alpha}{\partial \theta^2} =$

$\frac{\partial \rho_\alpha}{\partial \theta} = 0$).

After considering the assumptions above, simplification of the overall Equation (2.5)

gives

$$\frac{\partial \rho_\alpha}{\partial t} = -D_\alpha \left[\frac{1}{r}\frac{\partial}{\partial r}\left(r \frac{\partial \rho_\alpha}{\partial r}\right) + \frac{\partial^2 \rho_\alpha}{\partial z^2}\right] \tag{2.6}$$

Replacing ρ_α with concentration (C) of species α where $\rho w_\alpha = \rho_\alpha = C$, Equation (2.6)

becomes,

$$\frac{\partial C}{\partial t} = D_\alpha \left(\frac{1}{r}\frac{\partial}{\partial r}\left(r \frac{\partial C}{\partial r}\right) + \frac{\partial^2 C}{\partial z^2}\right) \tag{2.7}$$

A way to simplify Equation (2.7) is to nondimensionalize it by scaling. Scaling is important to figure out the sensitive parameters of the process and minimize the number of parameters. Introducing the following nondimensionalized forms, $C_s = \frac{C - C_{min}}{C_{max} - C_{min}}$, $t_s = \frac{t}{\frac{L^2}{D_\alpha}}$ where, L is the diffusion length considered to be half of the disk thickness, $r_s = \frac{r}{R}$, R is the disc radius, and $z_s = \frac{z}{L}$ into Equation (2.7) gives,

$$\frac{\partial C_s}{\partial t_s} = \left(\frac{L}{R}\right)^2 \frac{1}{r_s}\frac{\partial}{\partial r_s}\left(r_s \frac{\partial C_s}{\partial r_s}\right) + \frac{\partial^2 C_s}{\partial z_s^2} \tag{2.8}$$

The experimental gel disks used for diffusion have considerably larger radii than their thicknesses (L << R). The gel disks have L/R ~ 1/15[10]. Therefore, the value for the $\left(\frac{L}{R}\right)^2$ part of the equation becomes insignificant compared to the z-direction diffusion component $\frac{\partial^2 C_s}{\partial z_s^2}$. As a result, Equation (2.8) transforms from a two-dimensional equation to a one-dimensional equation describing diffusion in the z-direction only,

$$\frac{\partial C_s}{\partial t_s} = \frac{\partial^2 C_s}{\partial z_s^2} \tag{2.9}$$

To solve this differential equation, two boundary conditions and one initial condition are required. The initial condition can be set at time, t = 0, concentration of species α in the gel at any z location is C_0.

$$C(z, t = 0) = C_0 \tag{2.10}$$

Scaling analysis of the initial condition using the same spatial, time, and concentration scales results in the following condition

$$C_{s,}(z_s, 0) = 1 \qquad (2.11)$$

The first boundary condition states that species α is diffusing outwards. So, the concentration gradient at the center of the gel for species α will be zero,

$$\left.\frac{\partial C}{\partial z}\right|_{(0,t)} = 0 \qquad (2.12)$$

Expressing it into nondimensionalized format gives,

$$\left.\frac{\partial C_s}{\partial z_s}\right|_{(0,t_s)} = 0 \qquad (2.13)$$

The second boundary condition states that the amount of species α going out of the gel via diffusion at the gel boundary ($z = L$) will be equal to the convective removal of α from the gel boundary to the bath. Therefore,

$$D_\alpha \frac{\partial C(L,t)}{\partial z} = -h[C(L,t) - C_\infty] \qquad (2.14)$$

where, h is the convective mass transfer coefficient, and C_∞ is the concentration far away from the gel disk. Scaling this equation gives,

$$\frac{\partial C_s(1,t_s)}{\partial z_s} = -Bi C_s(1, t_s) \qquad (2.15)$$

where Bi is the Biot number which is the ratio of internal diffusion resistance to external convection resistance. Since the experiment is done in a well stirred bath, the external convection resistance becomes very low which will make the Biot number very large ($Bi \gg 1$). As a result, Equation (2.15) becomes,

$$C_s(1, t_s) = 0 \qquad (2.16)$$

From Equation (2.15) and (2.16), it can be observed that at the boundary, the rate of change in concentration of α is instant, and the concentration of α in the bath is not altered. It can be thought of an "infinite sink" with C_s being zero.

The resulting scaled solution for the system described above is as follows:

$$\frac{m}{m_0} = \int_0^1 \left\{ \sum_{n=1}^{\infty} \left[\frac{4(-1)^{n+1}}{\pi(2n-1)} \right] exp\left[-\left(\frac{(2n-1)\pi}{2} \right)^2 t_s \right] cos\left[\frac{(2n-1)\pi}{2} z_s \right] \right\} dz_s \qquad (2.17)$$

where m is the mass of species α at a given time and m_0 is the initial mass of species α. The contribution of terms in the summation decrease with increasing n and so we use the first five terms only as the approximate solution. The unscaled approximate solution becomes

$$\frac{m}{m_0} = \sum_{n=1}^{5} \left[\frac{4(-1)^{n+1}}{\pi(2n-1)} \right] exp\left[-\left(\frac{(2n-1)\pi}{2} \right)^2 \frac{tD_\alpha}{L^2} \right] \frac{2}{(2n-1)\pi} sin\left[\frac{(2n-1)\pi}{2} \right] \qquad (2.18)$$

The approximate solution is used to model experimental data to provide diffusivity of α (*i.e.*, AOT) using the fittype function in MATLAB[1]. After obtaining this diffusivity value, we can compare it with theoretical models.

2.5 Effects of Temperature on Diffusion in Gels

It is well known that increasing the temperature of a system increases the kinetic energy of its molecules and consequently increases their respective rates of diffusion. A fundamental parameter used to describe these temperature dependencies is the activation energy associated with each process. Diffusion activation energy will be investigated in this research for multiple polymer/solvent systems. The definition and the importance of diffusion activation energy will be discussed in the following paragraphs.

In a gel containing polymer, solute and a solvent, diffusion of the solute requires it to overcome an energy barrier that is called diffusion activation energy. Solute molecules begin diffusing after they achieve the required activation energy[25]. Activation energy of a solute in a specific gel can depend on polymer concentration[24,26], size of the solute[23,27,28], interaction between the gel and solute[23,27,28], and viscosity of the solvent used to make the gel[29].

Investigating diffusion activation energy of a solute in gels can have diverse objectives. For example, comparison between activation energy in gels varying in concentration and in pure solvent provide information about how the polymer in the gel impacts diffusion. Hendrickx *et al.*[30] found that diffusion of glucose in carrageenan gels is primarily impacted by the obstruction effect of the polymer. Finally, determining the dependence of activation energy with polymer concentration can provide understanding on interactions between the solute and the polymer[23]. Kwak *et al.* analyzed diffusion activation energies for multiple solutes in curdlan gels of different concentrations[23]. They concluded that since the solutes' diffusion activation energies do not change with polymer concentrations, the solutes had no interaction with curdlan polymer.

There are only a few diffusion models that consider diffusion at variable temperatures[31]. Two thermodynamic models that consider temperature-dependent diffusion will be discussed in the following sections. These models will be used to analyze the diffusivities obtained at various temperatures.

For physicochemical phenomena such as diffusion, electrical conductivity and viscosity etc. that involve transport, the general Arrhenius equation is commonly used to express the variation of the phenomenon against the reciprocal absolute temperature[32].

$$D = D_{inf} \exp\left(-\frac{E_A}{RT}\right) \qquad (2.19)$$

where D is the diffusion coefficient, D_{inf} is the theoretical diffusivity at infinite

temperature ($T \rightarrow \infty$), E_A is the diffusion activation energy, R is the gas constant and T is

absolute temperature.

The general Arrhenius model provides diffusion activation energy in a gel of fixed

polymer concentration. The diffusion activation energy of the solute can be obtained by

plotting the logarithm of D versus 1/T using an Arrhenius equation (Equation 2.19).

Although the general Arrhenius model has been shown to describe diffusion as a function

of temperature well, it is a generalized approach that lacks details necessary to relate

diffusivity to solute size or to the polymer networks[31].

Petit *et al.*[33] used diffusion activation energy in a model to provide relation between

polymer concentration, molecular size of the solute, temperature and self-diffusion

coefficients of the solute in a gel. This model provides the diffusion activation energy of

a solute in gels having a certain range of polymer concentration. According to their

model, the gel consists of a statistical network having an average mesh size, ξ. The solute

is considered to reside temporarily in a cavity within this mesh structure. To diffuse, the

solute has to overcome a certain energy barrier and jump to the next cavity (Figure 2.4).

In this model, one-dimensional diffusion occurs as a result of a series of jumps of the

solute. Also, the energy potential is considered periodic and of equal value, and the

interval between each jump is ξ.
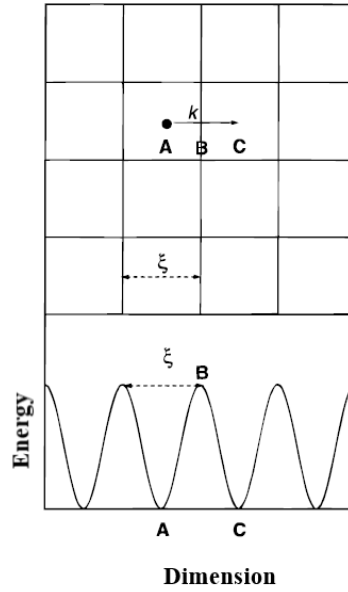
Figure 2.4: A gel having a statistical network of mesh size ξ and activation energy for the diffusion of a solute through a gel. Ref. taken from 33.

Andreoli *et al.*[34] related jump frequency, k, which is the rate at which the solute jumps from position A to C due to Brownian motion, with diffusivity as

$$D = \xi^2 k \tag{2.20}$$

The jump frequency is expected to depend on temperature and the size of the solute. It should also depend on polymer concentration but for simplification in the Petit model it is assumed to be constant over a certain concentration range. The jump frequency can be written in an Arrhenius form[35]

$$k = F_p \exp\left(-\frac{E_A}{RT}\right) \tag{2.21}$$

where F_p is a frequency prefactor, E_A is the activation energy, and T is the temperature.

The aforementioned mesh size, ξ can be calculated as[36]

$$\xi = R_g \left(\frac{c^*}{c}\right)^\nu \tag{2.22}$$

where R_g is radius of gyration of the polymer, c^* is the overlap concentration, c is the polymer concentration in the gel, and ν is a constant for a given system and depends only on the quality of the solvent. Substituting Equation (2.22) into (2.20), we get

$$D = R_g{}^2 \left(\frac{c^*}{c}\right)^{2\nu} k \tag{2.23}$$

Equation (2.23) becomes invalid as concentration approaches the overlap concentration. Therefore, Petit *et al.* formulated a better expression for D based on the friction coefficient of the diffusing molecule. The total friction coefficient f experienced by a diffusing solute can be divided into two contributions – contribution from the solvent background (f_0) and contribution from the polymer network (f_p)[37,38]

$$f = f_0 + f_p \tag{2.24}$$

After applying Stokes Einstein relation ($D_0 = k_B T/f_0$) and using Equation (2.20), Equation (2.24) can be written as

$$\frac{1}{D} = \frac{1}{D_0} + \frac{1}{k\xi^2} \tag{2.25}$$

where D_0 is the diffusion coefficient of the solute in solvent devoid of polymer.

The model of Petit et al. has been successfully used to describe the temperature dependence of solute diffusion in various polymer solvent systems[31,33]. For our gel systems we will use a modified version of this model described in Chapter 5.

2.6 Superposition Models

In this research, temperature dependent diffusivity of a solute through multiple types of polymer gels were measured over the temperature range of *ca.* 20°C to 40°C. Higher temperatures could not be explored due to experimental limitations. For example, our gels disintegrate at temperatures above 40°C in the mineral oils that we use to measure the diffusivities, making it impossible to measure the diffusivity above that temperature. Note, the gels are stable at much higher temperature in a system without the oil. Therefore, to broaden this narrow range over which diffusivity can be measured, an idea similar to the time-temperature superposition principle (tTSP), which is briefly explained below, was explored.

Using the time-temperature superposition principle, properties of linear viscoelastic materials can be obtained in cases when they cannot be measured. For example, using the model it can be determined how much deformation a material would go through over thirty years. In these extreme cases, tTSP can be used as a powerful tool that provides an estimation of properties. The idea behind this principle is that a change in polymer deformation rate is equivalent to a change in temperature. According to the tTSP, measuring short term creep responses of a material at various temperatures provides a master curve obtained by shifting the response curves using a horizontal shift factor. This master curve provides creep responses over a larger range of time[39]. In Figure 2.5, T_1 through T_5 curves represent response curves obtained over short period of times at various temperatures (T_1 to T_5). Taking the T_1 curve as the reference curve, shift factors, α_T (obtained via various theory), are used to shift the T_2-T_5 curves. The shifting provides the master curve shown in Figure 2.5. In this thesis a similar concept will be used to

broaden the temperature range over which diffusivity – a time-based phenomenon – is

measured through a concept we refer to as composition-diffusion superposition. In this

model, we hypothesize that a change in solvent composition has an equivalent change in

viscosity, which subsequently affects solute diffusivity. The details about our model is

provided in Chapter 5.2.
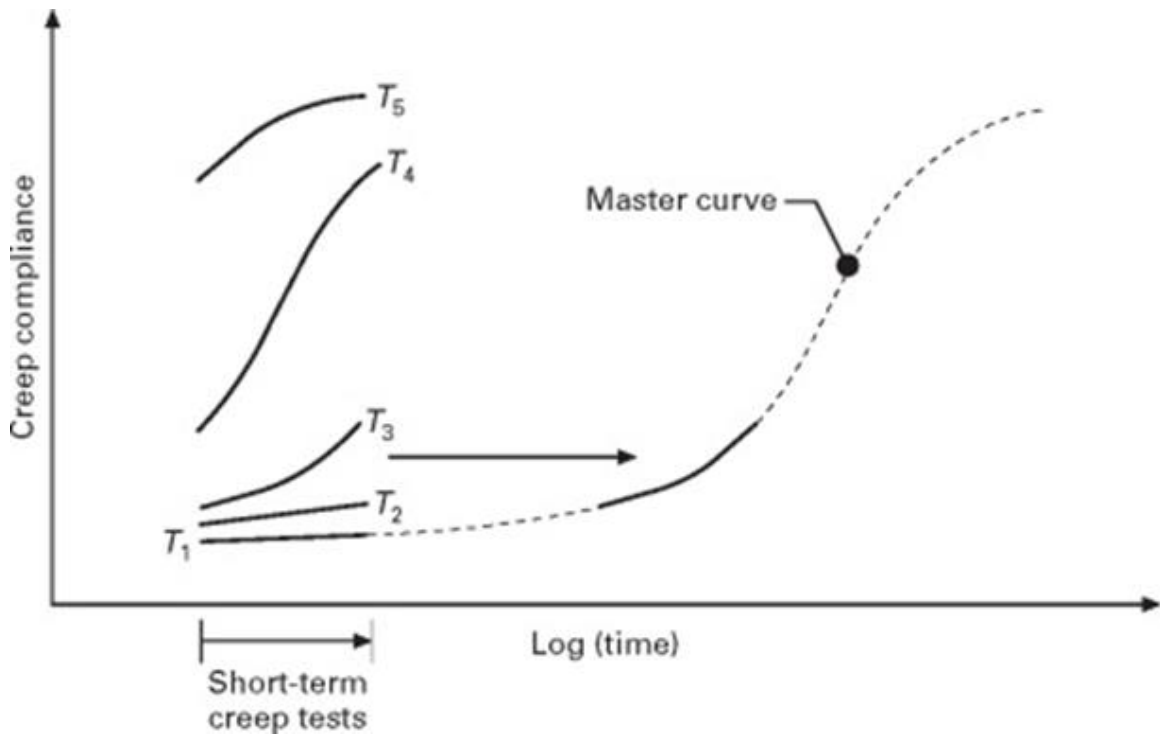
Figure 2.5: Creep compliance vs. log (time). Ref. taken from 39

3. Experimental Section

3.1 Experimental Setup

The experimental setup (Figure: 3.1a,b) for the diffusion experiment included a temperature-controlled recirculating bath, a shaker table, an aluminum manifold capable of housing five sample enclosures each with the capacity to hold gel samples and supernatant mineral oil, and a thermocouple. Liquid from the recirculating bath flowed through the manifold to control the mineral oil temperature inside the sample enclosures. The manifold was mounted on a shaker table to continuously agitate the samples. The thermocouple continuously recorded the temperature of oil inside a particular sample enclosure. Throughout each experiment, the location of the thermocouple was changed to capture the variation in oil temperature at different sample enclosure positions. There was negligible temperature variation across the different sample enclosures. The manifold and corresponding tubing were insulated to reduce heat loss to the surrounding. The actual temperature inside the sample enclosure was calibrated based upon the temperature set point of the recirculating bath and the two were found to differ slightly. A calibration plot (Figure 3.1c) showing this variation is provided below.
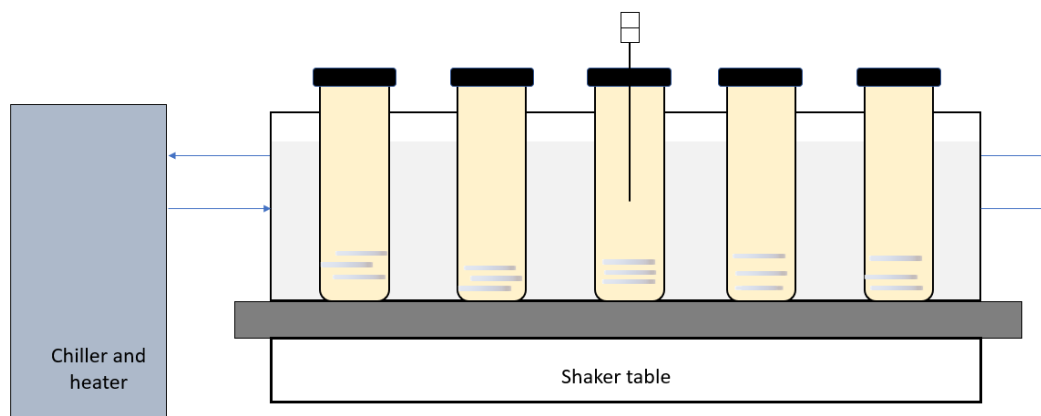
(a)

(b)
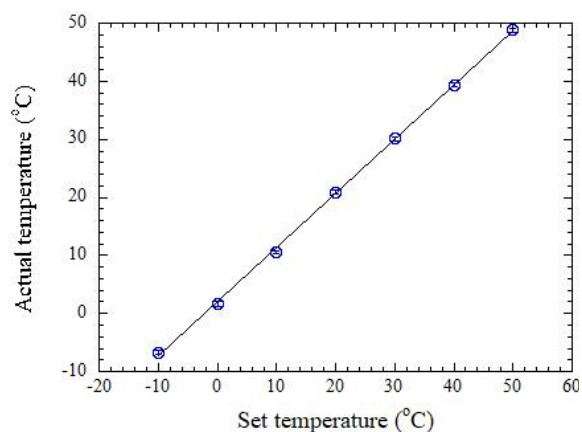
(c)

Figure 3.1: Experimental setup for the diffusion experiments (a), a photo of the actual

setup (b), calibration plot for actual temperatures at various temperature set points of

the recirculating bath (c) where the line is a linear fit.

3.2 Materials and preparation

Three types of organogels were fabricated. Each type contained one of the three mineral

oils – Hydrobrite 380 (HB 380) (Sonneborn LLC, Petrolia, PA, USA), Hydrobrite 200

(HB 200) (Sonneborn LLC, Petrolia, PA, USA) and Squalane (SQ) (98% pure, Alfa

Aesar, Ward Hill, MA, USA), and copolymer poly[styrene-b-(ethylene-co-butylene)-b-styrene] (SEBS) supplied by Kraton Polymers LLC, Houston, TX, USA (G1654 grade, 158 kg/mol and $f_S = 0.278$ g S/g). All of the gels contained aerosol-OT (AOT, >97% pure, Sigma Aldrich, St. Louis, MO, USA) as a diffusion probe.

To prepare the gels, desired quantities of respective polymer, oil and AOT were dissolved in toluene. The ratio of toluene volume to total mass of all the gel components were 20:1. For example, 4 g polymer, 15.8 g oil, and 0.2 g AOT were dissolved in 400 mL of toluene. The mixture containing gel components and toluene was stirred on a stir plate until a homogeneous solution was formed. Then, toluene was removed from the solution using a rotary evaporator and the subsequent gel products were annealed in a vacuum oven at 140 °C and 27 inHg vacuum for 18 hours. After annealing, the gels were shaped into disks (diameter 25mm and thickness 1.65mm) using a Carver Press at temperatures varying with total polymer concentration. The gel disks were preswollen in their respective solvent containing 1 wt% AOT (e.g., for a gel made of SEBS, HB 200, and 1 wt% AOT, the preswelling solution contained HB 200 with 1 wt% AOT). All of the above-mentioned types of gels were prepared for five different formulations (~10 wt%, 15wt%, 20 wt%, 25 wt%, 30 wt% polymer) initially, and after preswelling polymer concentrations were reduced. For example, initially a gel made with HB380 and SEBS had ~10 wt% SEBS, and after preswelling SEBS concentration reduced to 6.8 ± 0.01 wt% (Table 3.1). A summary of final (*i.e.*, preswollen gel) SEBS concentrations for all of the gels is provided in Table 3.1.

Table 3.1: SEBS concentration in the gels after preswelling based on solvent and concentration before preswelling occurred.

Solvent	SEBS concentration before preswelling				
	10 wt%	15 wt%	20 wt%	25 wt%	30 wt%
HB380	6.8 ± 0.01	8.8 ± 0.03	10.9 ± 0.05	13.2 ± 0.03	15.3 ± 0.09
HB200	6.2 ± 0.00	8.4 ± 0.00	10.5 ± 0.01	12.7 ± 0.04	14.5 ± 0.01
SQ	7.1 ± 0.02	9.4 ± 0.1	11.7 ± 0.02	14.0 ± 0.04	16.3 ± 0.00
Average	6.7	8.9	11.0	13.3	14.8

3.3 Viscosity measurements

The viscosities of HB 200, HB 380 and Squalane were measured over the temperature range of 10 °C to 70 °C using a Brookfield (Middleboro, MA, USA) DVE viscometer with a small sample adapter. The instrument was connected to a temperature-controlled recirculating bath from which the recirculating liquid was pumped through the small sample adapter jacket to control its temperature. Viscosity measurements were taken after 30 minutes of equilibration time to ensure the solvent reached the desired temperature. Measurements were repeated three times to ensure reproducibility. The measurements were done in both the heating (from 10 °C to 70 °C) and cooling (from 70 °C to 10 °C) directions to make sure that the 30 minutes equilibration time was adequate. The spindle speed and equilibration time for each measurement varied according to the oil under investigation and also the temperature (for example, for measurements at lower temperatures and higher viscosity oils, the speed should be lower so that the load bearing capacity of the instrument stays within 10-100% of the transducer range).

3.4 Diffusion experiments

After taking initial measurements of AOT concentration in the preswollen gels using Fourier transform infrared (FTIR) spectroscopy, they were submersed in their respective gel solvent in its pure form (*i.e.*, without any AOT). Triplicate gel samples of each composition were submersed in a sample enclosure containing 100mL oil. Sample enclosures were fixed to a shaker table, which was maintained at 200 rpm throughout all diffusion experiments. Gels were periodically removed from each sample enclosure, gel surfaces were wiped of any residual mineral oil, and the mass and AOT concentration were measured using a gravimetric scale and FTIR, respectively. Gels were returned to their respective sample enclosure after each measurement. Diffusion experiments were conducted for five different compositions of each organogel type at five different temperatures ranging from ca. 20 °C-40 °C using the experimental setup explained above. The FTIR instrument used in this analysis was a Thermo Scientific Nicolet iS10 spectrometer and was purged with N_2 during experiments. A spectral resolution of 0.5 cm^{-1} and an average of 32 scans were used for each spectrum.

4. Results

In this research, we measured diffusivity values of AOT reverse micelle in three types of gels. Each type of gel contained SEBS copolymer, AOT reverse micelle and one of the three mineral oils – HB 380, HB 200 and SQ. For each gel type, diffusivities in five different concentrations at five different temperatures were determined. The obtained results are presented in Figure 4.3 at the end of this chapter. To measure the diffusivity values, a method[1] involving FTIR spectroscopy established by Mineart *et al.* was utilized. The method of determining the diffusivities will be explained below.

As described in Chapter 2, SEBS and mineral oil gels form organogels that have glassy polystyrene domains and a continuous midblock/solvent region. AOT reverse micelles reside in the latter region and diffuses through that region. AOT reverse micelle contains carbonyl groups that are tracked at various times using FTIR spectroscopy to provide the diffusivity data. During the diffusion experiment, the peak representing carbonyl stretching (1739 cm^{-1}) goes down with time as the AOT reverse micelle concentration decreases (Figure 4.1). Some important FTIR peaks for our gels are presented in Table 4.1.
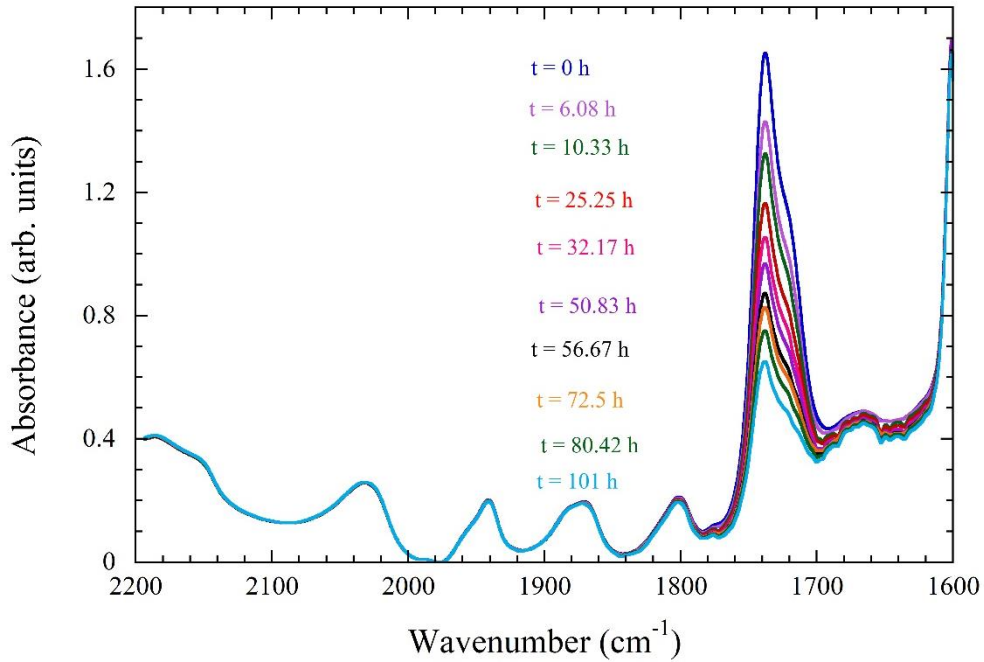
Figure 4.1: FTIR spectra of AOT reverse micelle diffusion at 30 °C in a gel containing 10.5 wt% SEBS and HB200. The peak at 1739 cm⁻¹ is tracked with time to determine the AOT reverse micelle diffusivity.

Table 4.1: FTIR peaks for functional groups present in our gels

Functional group	FTIR peak (cm⁻¹)
Carbonyl (AOT)	1739
Phenyl (SEBS)	1940
Phenyl (SEBS)	1870
Phenyl (SEBS)	1800
Phenyl (SEBS)	1745

Equation (2.18) is used to determine the diffusivity values. and requires retained mass data to calculate diffusivity. Retained mass $\frac{m}{m_0}$ of AOT reverse micelles was obtained by

tracking the carbonyl peak absorbance at 1739 cm^{-1}. The peak absorbance can be correlated to the AOT concentration in the gel using Beer's law.

$$A = l \sum_i \varepsilon_i c_i \qquad (4.1)$$

where A is absorbance, l is path length, ε_i is the molar absorptivity, and c_i is the concentration of species i.

It should be noted that the peak height obtained at 1739 cm^{-1} also has a contribution from a phenyl group (at 1745 cm^{-1}) from SEBS. This contribution from the phenyl group is removed by incorporating a correction factor during the calculations. For each gel formulation undergoing diffusion, a control was prepared and preswollen that did not have any AOT reverse micelle. The peak height in those samples at 1739 cm^{-1} was the contribution from the phenyl group at 1745 cm^{-1}. The correction factor incorporated the path length difference between the control and samples, and the control peak height at 1739 cm^{-1}. The diffusivity values were calculated after subtracting the correction factor[1].

According to Equation (4.1) at time 0 and time t, the ratio of carbonyl peak absorbances can be written as

$$\frac{A_t}{A_0} = \frac{l_t \sum_i \varepsilon_{i,t} c_{i,t}}{l_0 \sum_i \varepsilon_{i,0} c_{i,0}} \qquad (4.2)$$

The path lengths in our samples are constant with time since these were preswollen before the diffusion experiment. Molar absorptivity of a certain species is also a constant. Therefore, Equation (4.2) can be written as

$$\frac{A_t}{A_0} = \frac{c_{i,t}}{c_{i,0}} \qquad (4.3)$$

Again, due to preswelling, the volume of the gel samples does not change during the

diffusion experiment. As a result, $\frac{c_{i,t}}{c_{i,0}}$ equals to $\frac{m_{i,t}}{m_{i,0}}$. So, absorbance and retained mass in

our gels are related as

$$\frac{A_t}{A_0} = \frac{m_{i,t}}{m_{i,0}} \tag{4.4}$$

The retained mass data corresponding to Equation 4.4 for gels containing 10.5 wt%

SEBS and HB200 at different temperatures is presented below (Figure 4.2). We observe

that the concentration of AOT reverse micelle decreases with time as expected. The

retained mass profile clearly demonstrates the impact of temperature on mass transport.

With the increase in temperature, the initial slopes of the plots become steeper. Thus we

find that for the same gel, mass transport at a lower temperature is much slower. This

observation is the same for all of the types of our investigated gels.
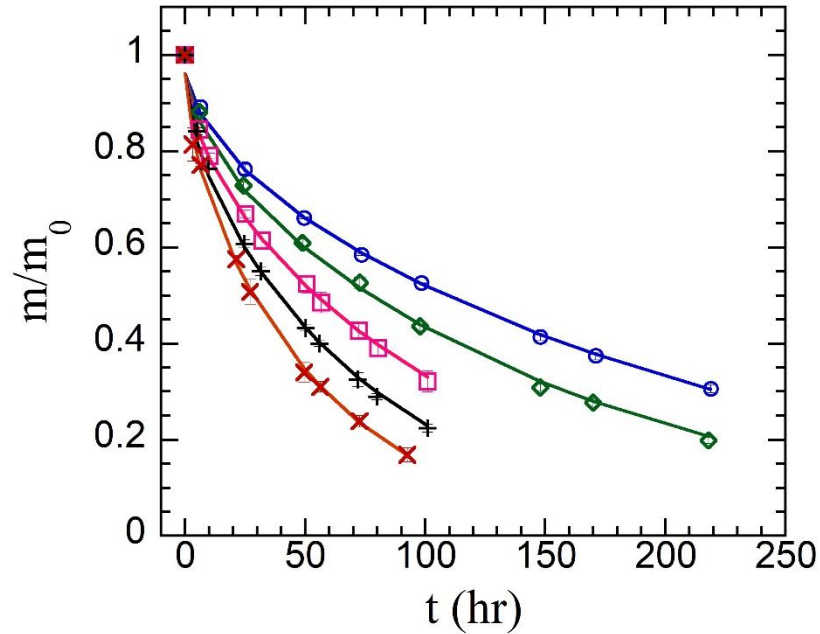
Figure 4.2: Average retained mass of AOT reverse micelle for the gel formulated with 10.5 wt% SEBS and HB200 at 19.6 ℃ (○), 24.7 ℃ (◊), 30.0 ℃ (□), 35.6 ℃ (+) and 40.2 ℃ (×). The solid lines represent Equation (2.18) for corresponding gels.

Goal I of this research was to quantify the diffusivity of AOT reverse micelle through gels with different copolymer concentrations and solvent viscosity for a range of temperatures. This goal was achieved in this chapter by obtaining the diffusivity values (Figure 4.3) from the retained mass profiles. We observed that for each type of gel diffusivity of AOT reverse micelle increases with the increase in temperature. We also observed that at a fixed temperature, diffusivity decreases as the polymer concentration increases. We further noted that at a fixed polymer concentration and temperature, diffusivity decreases with the increase in gel solvent viscosity (SQ < HB 200 < HB 380).
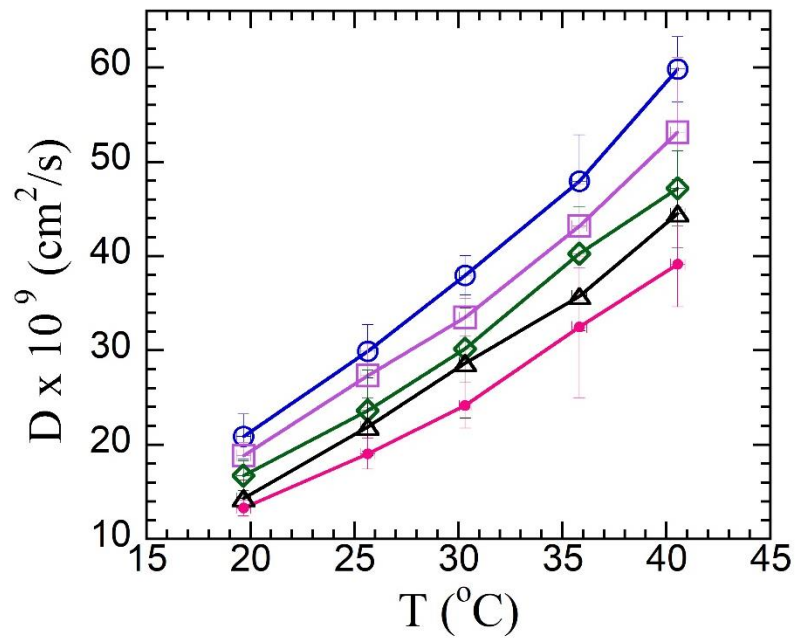
(a)
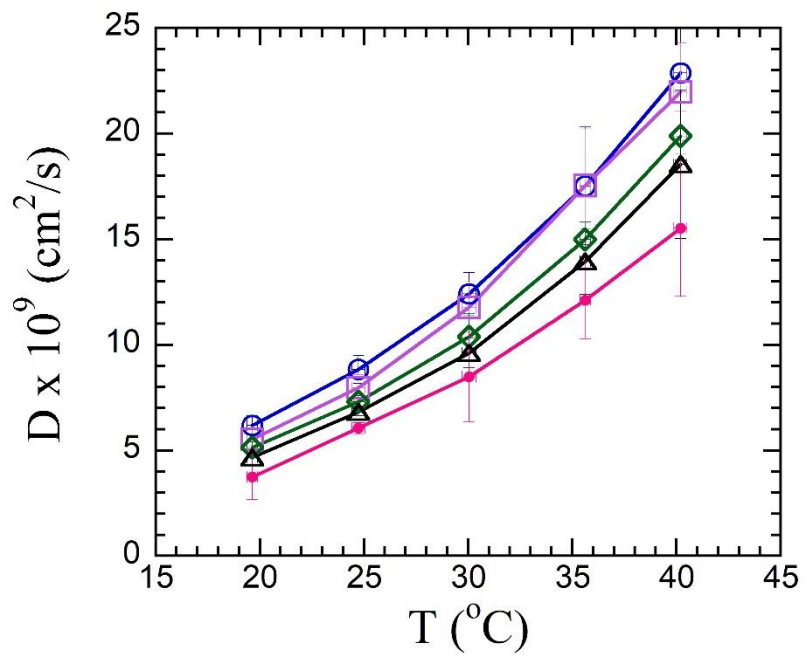
(b)
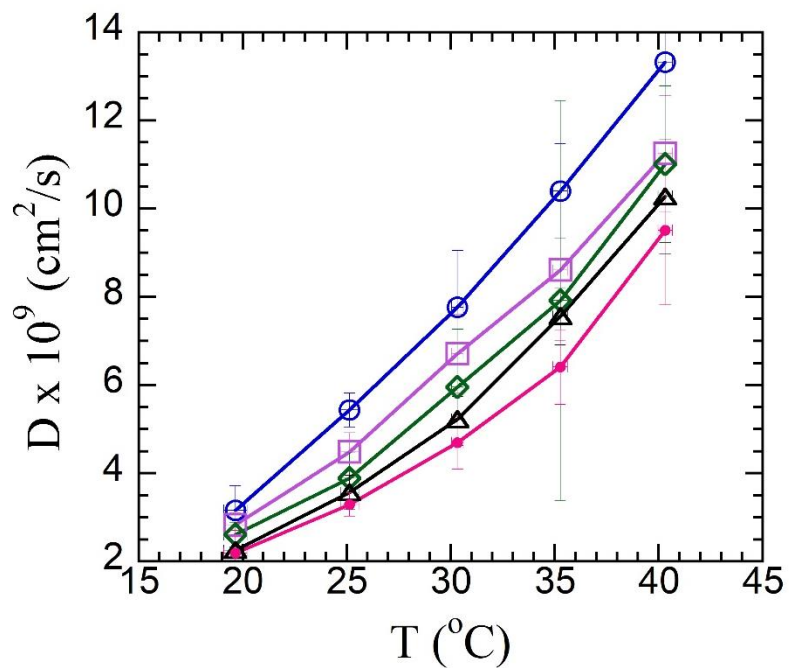
(c)

Figure 4.3: Diffusivity vs. Temperature data for (a) SEBS+SQ, (b) SEBS+200 (c) SEBS+380 at SEBS concentration 6.2-7.1 wt% (○), 8.4-9.4 wt% (□), 10.5-11.7 wt% (◊), 12.7-13.2 wt% (Δ), 14.5-16.3 wt% (●). The lines are guides to the eyes.

5. Discussion

5.1 Models for Diffusivity-Temperature Relation

To achieve Goal II of this research, this section seeks to better understand the temperature dependent diffusion behavior of AOT reverse micelles in organogels (data displayed in Figure 4.3) using existing theoretical models. The obtained temperature dependent diffusivity data were fitted with two different models – the general Arrhenius model and the detailed model derived by Petit *et al.* – to extract the diffusion activation energy of the solute in each type of gel.

5.1.1 General Arrhenius Model

The general Arrhenius model is a simple model that relates solute diffusivity to temperature without including detailed physical aspects of a system. The Arrhenius equation (Equation (2.19)) can be linearized in terms of the independent and dependent variables as

$$\ln(D) = \ln(D_{inf}) - \frac{E_A}{R}\left(\frac{1}{T}\right) \qquad (5.1)$$

Therefore, plotting $\ln(D)$ vs. $1/T$ (Arrhenius plot) will be linear in cases of polymer gels that follow the Arrhenius behavior. The slope $-\frac{E_a}{R}$ of the plot will provide the diffusion activation energy and the intercept will provide the theoretical solute diffusivity at infinite temperature.

Figure 5.1 presents $\ln(D)$ vs. $1/T$ plot for all of the gels. The R^2 values (all $\geq$0.985) for the plots indicate that the lines are good fits to Equation (5.1) and all of the gels follow the Arrhenius model.
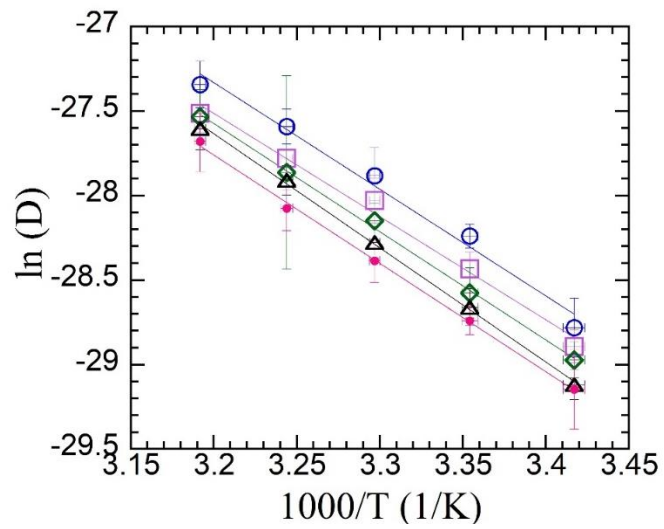
(a)
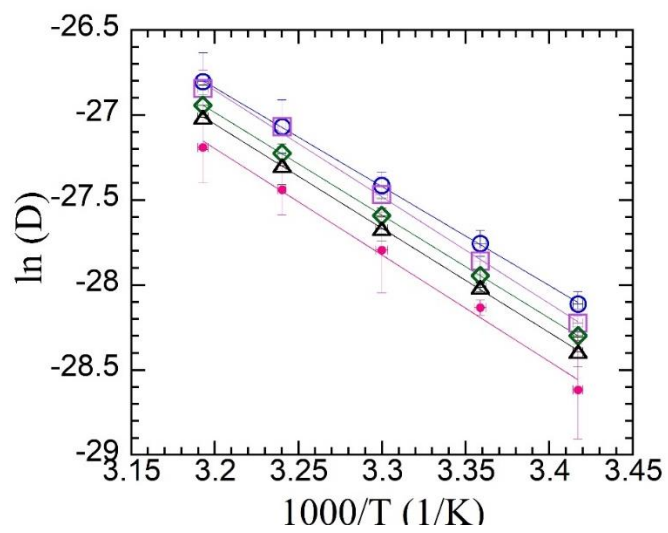
(b)
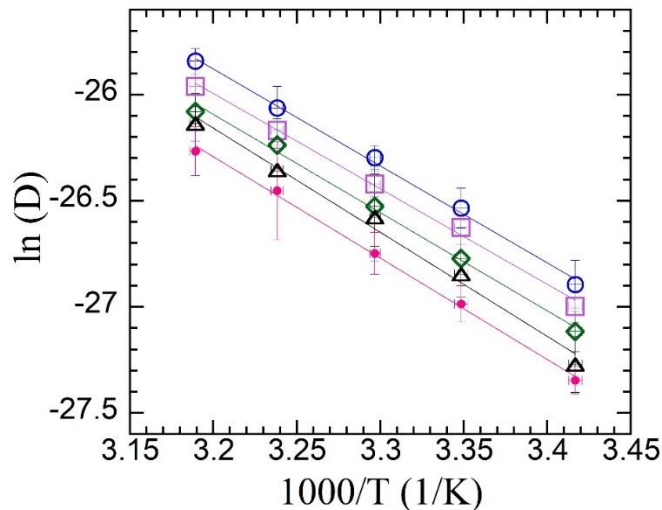
(c)

Figure 5.1: Arrhenius plots for gels made with SEBS and HB 380 (a) or HB 200 (b) or SQ (c) at SEBS concentration 6.2-7.1 wt% (○), 8.4-9.4 wt% (□), 10.5-11.7 wt% (◊), 12.7-13.2 wt% (Δ), 14.5-16.3 wt% (●). The lines are fit to Equation (5.1).

The viscosities of the gel solvents SQ, HB 200, HB 380 are 29, 80, 153 cP at 25°C, respectively. It is observed from Figure 5.2 (a) that the diffusion activation energy of the solute increases with the increase in gel solvent viscosity. This could be due to the increased drag on the solute caused by more viscous solvent in the gel. Moreover, increased solvent viscosity is likely the result of larger oil molecules and the hydrodynamic radius of the AOT solute can include several solute-bound solvent molecules. Therefore, another reason for the observed trend could be the increase in the hydrodynamic radius of the AOT solute in higher viscosity gels. There is more explanation on the impact of gel solvent viscosity on diffusivity in Section 5.2. It can also be noted from Figure 5.2 (a) that for a given gel type, within the investigated concentration range, diffusion activation energy of AOT reverse micelle remains

relatively constant as a function of polymer concentration in the gel. Therefore, it is observed from our gel systems that there is a lack of interaction between the AOT reverse micelles and copolymer midblocks.
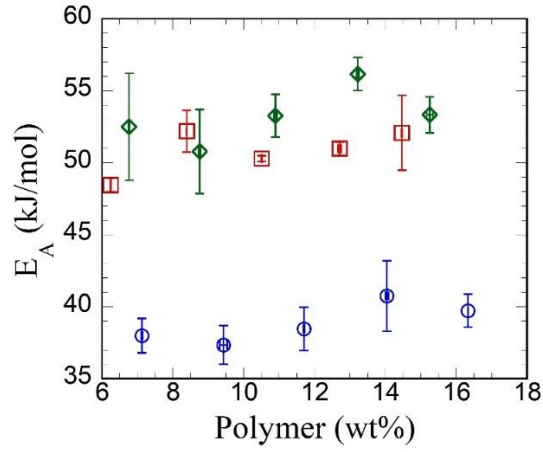
(a)
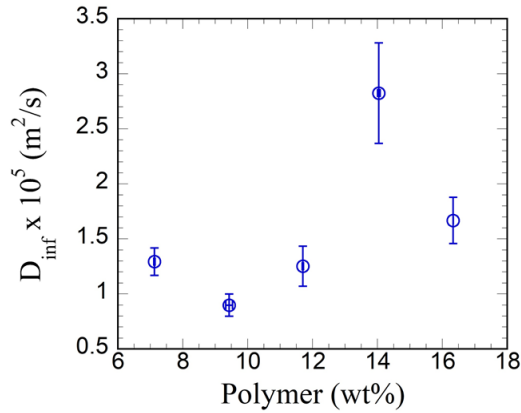
(b)
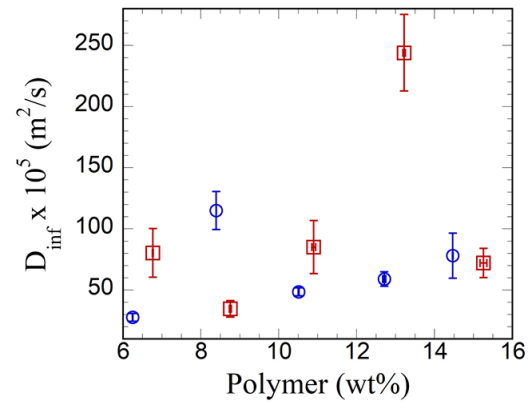
(c)

Figure 5.2: (a) Diffusion activation energy vs. polymer wt% for SEBS+SQ (○), SEBS+200 (□) and SEBS+380 (◊). Diffusivity at infinite temperature vs. polymer wt% for (b) SEBS+SQ and (c) SEBS+200 (○) and SEBS+380 (□). Linear regression was used to collect the fit parameters - E_A and $D_{inf.}$

In the Arrhenius model, there are two fitted parameters D_{inf} and E_A. Like the diffusivity versus copolymer concentration trend noted from Figure 4.3, we anticipate that diffusivity at infinite temperature should decrease with the increase in concentration. However, fitting each data set independently (*i.e.*, with its own E_A and D_{inf}) provides unclear interpretation of the parameter D_{inf} (Figure 5.2 b, c). Based on this, we decided to fit data with a single unified diffusion activation energy assuming the concentration independence of E_A (as proven in Figure 5.2 a) for all five of the concentrations of each type of the gels. The data are still well-described by this approach and unified E_A values (38.9 ± 0.7, 50.8 ± 0.6, 53.2 ± 1.0 kJ/mol for gels made with SQ, HB200 and HB380, respectively) are similar to those presented in Figure 5.2a. Additionally, D_{inf} values extracted using this approach follow the anticipated trend where for each type of gel D_{inf} decreases with the increase in polymer concentration (Figure 5.3).

(a)   (b)
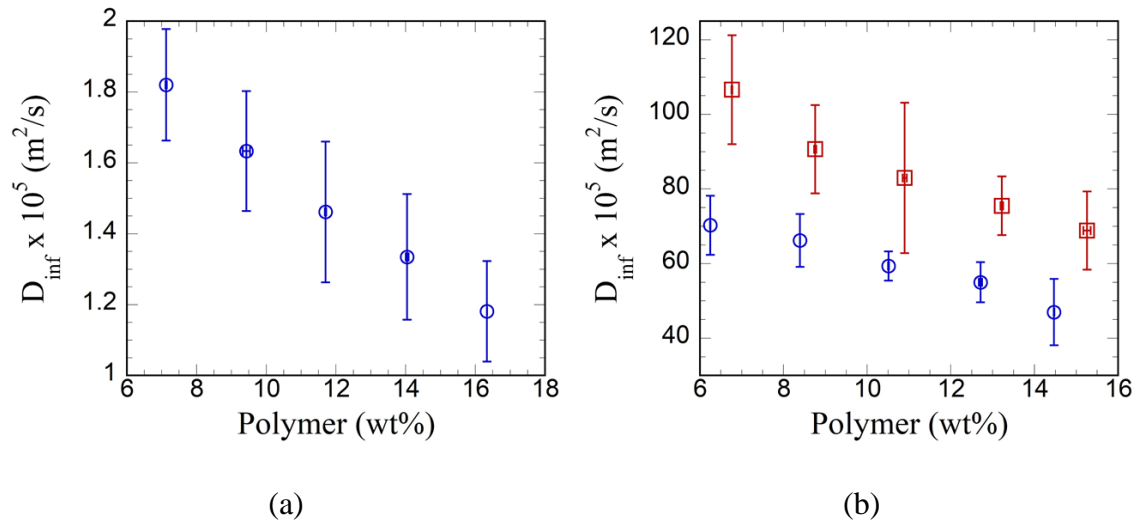
Figure 5.3: Diffusivity at infinite temperature obtained from the unified activation energy fitting vs. polymer wt% for (a) SEBS+SQ and (b) SEBS+200 (○) and SEBS+380 (□).

5.1.2 Petit et al. Model

The model of Petit[33] is a more complex model than the general Arrhenius one because it includes physically-relevant structural factors. Generally, the Petit model has been used to describe diffusion in gels with negligible crosslink size[33]. In our investigation of styrenic gels, polymer networks have crosslinks that are physically formed by glassy polystyrene domains (Figure 2.3) of 10-20 nm[9,40]. The polystyrene domains are impenetrable by the diffusing species. Hence, we have to account for the obstruction effect from the polystyrene domains in the gels while using the diffusion model of Petit.

The diffusion model based on obstruction effects by Mackie and Meares[41] was utilized along with the model of Petit to describe diffusion through our styrenic block copolymer organogels. Mackie and Meares considered that in the case of diffusion of a solute in a gel, polymer chain mobility is less significant than the diffusion of the solute. The polymer chains are motionless and impenetrable for the species diffusing. As a consequence, the polymer chains increase the path length for the diffusing species[31]. Diffusion occurs only through the sites unoccupied by the polymer chains. According to the Mackie and Meares model, in a gel, diffusivity of a small molecule through a polymer gel can be described as[21]

$$\frac{D_g}{D_0} = \left(\frac{1-\phi}{1+\phi}\right)^2 \tag{5.2}$$

where D_g is diffusivity in the gel and ϕ is the volume fraction of the polymer.

Zhang *et al.*[42] analyzed ionic conductivity of ion gels made with poly(styrene-b-ethylene oxide-b-styrene) (SOS) triblock copolymer over the composition range of 10-50 wt% of SOS and temperature range of 25-160 °C. In their ion gels, both the midblocks and the

ionic liquid (*i.e.*, gel solvent) form the conducting domain and the polystyrene domains are insulating causing the path length of the ions to increase. So, they considered the conducting phase as the 'solvent' in their analysis. They observed that the dependence of the ionic conductivity on the volume fraction of polystyrene complies well with the obstruction model developed by Mackie and Meares. As Zhang *et al.* analyzed ionic conductivity which is inherently diffusion of ions in a styrenic triblock copolymer, we mirror their approach and incorporated the Mackie and Meares model in our diffusivity analysis.

In our styrenic gels, solute diffusion occurs through the midblock/solvent region. We considered our gels' midblock/solvent region as the 'solvent' region. The Mackie and Meares model in case of our gels can be expressed as

$$\frac{D_g}{D_s} = \left(\frac{1 - \phi_S}{1 + \phi_S}\right)^2 \tag{5.3}$$

where D_s is the diffusivity of solute through the solvent (polymer solution analogous to the midblock/solvent matrix), and ϕ_S is the volume fraction of polystyrene in the gel.

According to the model of Petit, the diffusivity through our midblock/solvent matrix in the gel can be described by a combination of frictional forces from the solvent and polymer molecules

$$\frac{1}{D_s} = \frac{1}{D_0} + \frac{1}{k\xi^2} \tag{5.4}$$

Altogether, combination of the Mackie and Meares model and the model of Petit takes the form

$$\frac{\left(\frac{1-\phi_S}{1+\phi_S}\right)^2}{D_g} \equiv \frac{1}{D_{g,c}} = \frac{1}{D_0} + \frac{1}{k\xi^2} \tag{5.5}$$

where $D_{g,c}$ is referred to as the corrected solute diffusivity through the gel. In terms of preceding discussion up to this point, D_g is simply equal to our measured solute diffusivities D (Figure 4.3).

Before applying the Petit model, we must establish the impact of polymer concentration on gel mesh size. Diffusivities of AOT solute in organogels made with SEBS copolymer and one of the three mineral oils – HB 380, HB 200, or SQ – were studied where the gel mesh size was varied via copolymer concentration. Gel mesh size was calculated based on copolymer concentration using Equation (2.22)

$$\xi = R_g \left(\frac{c^*}{c}\right)^{\nu} \tag{2.22}$$

Because diffusion occurs only in the midblock/solvent region, only the midblock concentration within this region is considered in the calculations using Equation 2.22. The midblock EB concentration in the midblock/solvent region, c_{EB}, is calculated by

$$c_{EB} = \frac{w_{SEBS} f_{EB}}{\frac{w_{EB}/\rho_{EB}}{MO} \frac{MO}{MO}} \tag{5.6}$$

where w_{SEBS} is the mass fraction of SEBS in the gel, f_{EB} is mass fraction of midblock in SEBS, $w_{EB/MO}$ is the total mass fraction of midblock and mineral oil in the gel, and $\rho_{EB/MO}$ is the density of midblock/solvent region.

For all of the investigated gels, the solvents are good solvents for the respective polymer. So, the value of ν is kept as a constant value of 0.588 as it is the established value of the Flory exponent for a good solvent[36]. Details for mesh size calculations are provided in Appendix A. As an example, a SEBS gel with the specific copolymer used here (R_g = 12.7 nm, $c^* = 0.022$ g/cm^3) with 6.8 wt% SEBS, has a mesh size of 8.4 nm (8.4 x 10^{-7} cm).

The volume fraction of polystyrene, ϕ_s in our SEBS gels is calculated as[10]

$$\phi_S = \frac{w_{SEBS} \times f_s \times \rho_{gel}}{\rho_S} \tag{5.7}$$

where f_s is the mass fraction of polystyrene in SEBS, ρ_{gel} and ρ_s are the densities of the gel and polystyrene, respectively.

Our experimental diffusivity data were fitted with the Petit model (Figure 5.4), and the R^2 values indicate a good fit. According to Equation (5.5), plotting $\frac{1}{D_{g,c}}$ vs. $\left(\frac{1}{\xi^2}\right)$ should provide a straight line with intercept $\frac{1}{D_0}$ and slope $\frac{1}{k}$. D_0 and k were obtained as fitting parameters (using linear regression from Figure 5.4 data). D_0 values are provided in Figure 5.5. It is observed from the figure that D_0 is a function of temperature and increases with the increase in temperature as anticipated because increased temperature increases the kinetic energy of the solvent molecules increasing their diffusion rate.

(a)

(b)

(c)
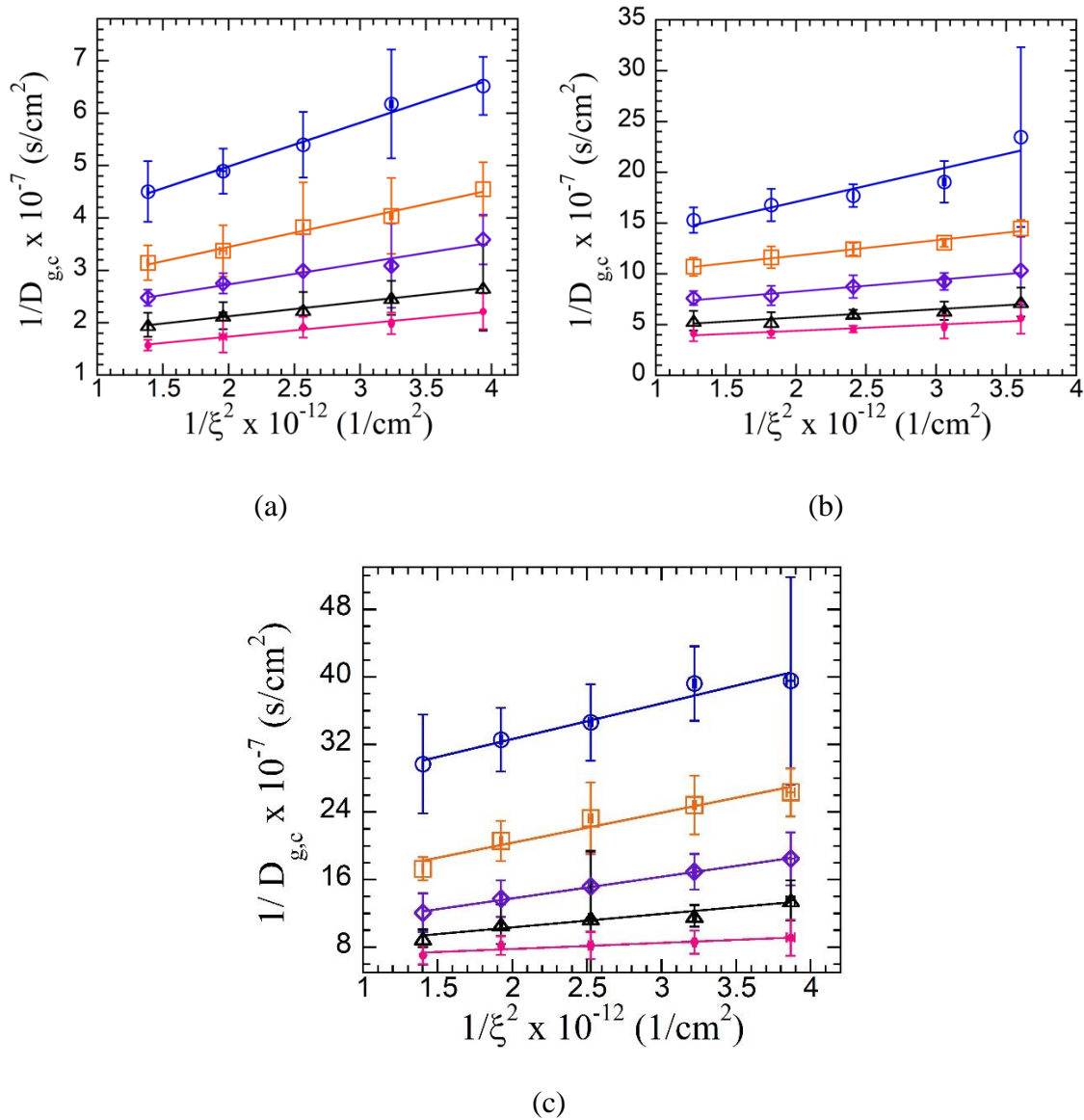
Figure 5.4: (a) Plots to extract D_0 and k for SEBS+SQ (a), SEBS+200 (b) and

SEBS+380 (c). Solid lines are linear fits. (○), (□), (◊), (Δ) and (●) represents

temperatures ~ 19.7, 25.2, 30.2, 35.6, 40.3 °C, respectively. R^2 is ≥ 0.96 for all (a),

R^2 is ≥ 0.91 for 25.2, 30.2, 35.6 °C series and ≥ 0.88 for the other two series (b), R^2

is ≥ 0.92 for 19.7, 25.2, 30.2, 35.6 °C series and 0.87 for 40.3 °C (c).

According to the assumption made in the model of Petit, k is considered constant over a certain concentration range and depends only on the temperature and the solute size. In our investigation, k was found to increase with the increase in temperature (Figure 5.6) for all types of gels.

The equation relating the jump frequency and diffusion activation energy (Equation 2.21) can be rewritten as

$$lnk = \ln F_p - \left(\frac{E_A}{R}\right)\frac{1}{T} \tag{5.8}$$

The slopes of ln*(k)* vs. *1/T* linear plots provide the diffusion activation energies of AOT reverse micelle in case of all of the gel systems (Figure 5.6). The R^2 values (all ≥0.91) for the linear fits of the plots indicate that the lines are a good fit to Equation (5.8). The activation energies obtained from the slope $\left(\frac{E_A}{R}\right)$ were found to be 46.8 ± 3.0 kJ/mol, 57.5 ± 6.6 kJ/mol and 63.5 ± 11.6 kJ/mol for SEBS+SQ, SEBS+HB200 and SEBS+HB380 gels, respectively.
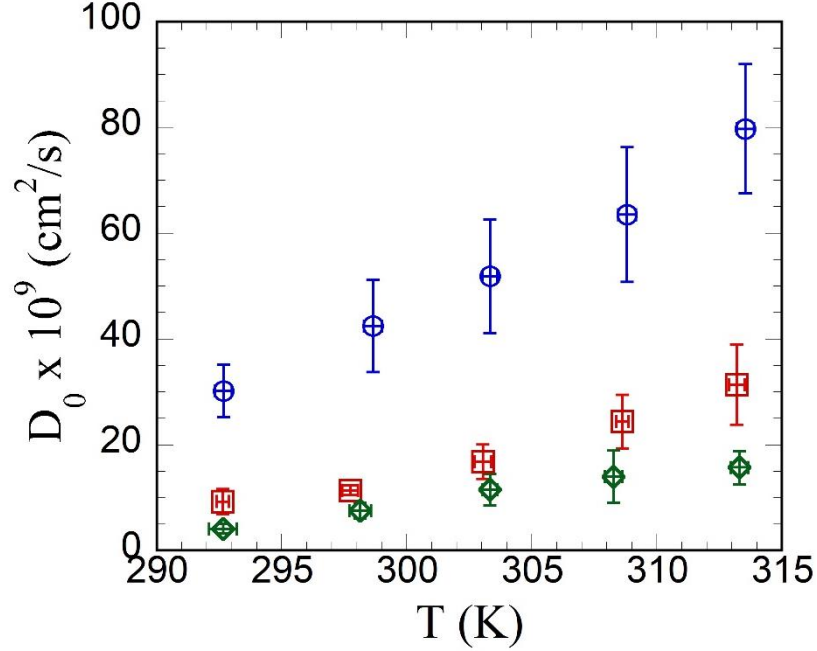
Figure 5.5: Diffusivity in solvent devoid of any polymer vs. temperature for

SEBS+SQ (○) SEBS+200 (□) and SEBS+380 (◊).

The hydrodynamic radius, r_h of AOT reverse micelle was calculated for our all three

types of gels using the Stokes-Einstein equation

$$r_h = \frac{k_B T}{6\pi\mu D_0} \tag{5.9}$$

where k_B is the Boltzmann constant, T is the absolute temperature, μ is the solvent

viscosity and r_h is the hydrodynamic radius of the solute. Karver *et al.* found the value of

the hydrodynamic radius of AOT reverse micelle to be ≈1.7 nm in dodecane using

transient current measurements[43]. In our gels, the calculated values of the hydrodynamic

radii were found to be 2.0 ± 0.5, 2.1 ± 0.4, 1.8 ± 0.3 nm from SEBS+HB 380, SEBS+HB

200 and SEBS+SQ gels, respectively. The similarity of the hydrodynamic radius between

the literature value and the calculated values using the fit parameter, D_o from the Petit

model further strengthens the Petit model's validity for our gel systems.
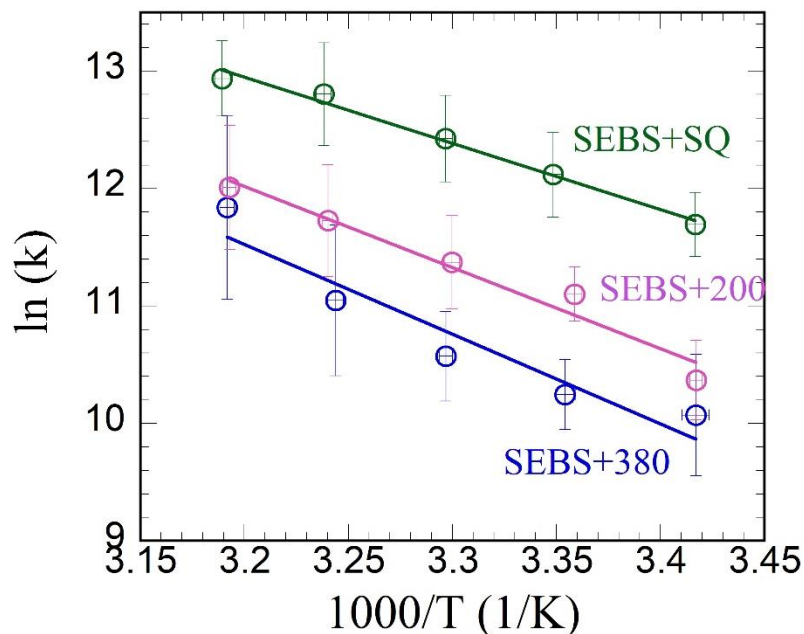
Figure 5.6: Arrhenius plot based upon jump frequency for different gels. The lines are

fits using Equation 5.8.

5.1.3 Comparison of Models

We want to reemphasize that the general Arrhenius model is a simpler model describing a

temperature dependent phenomenon and it does not include any fine details about our

system such as polymer mesh size, crosslink size and solute penetrability. On the other

hand, the Petit model is a significantly complicated model that accounts for the different

aspects of the heterogeneity of our systems by considering the glassy polystyrene

domains, polymer chains and the hopping of solute through the mesh. Hence, we can say

that the Petit model represents our gel system more accurately. The activation energy

values (unified activation energy) found from the general Arrhenius model are

statistically lower (for all cases $p < 0.05$, from t-test) than the activation energies obtained

from the model of Petit for all types of gels (Figure 5.7). Kwak *et al.* found a similar

trend in their investigation of activation energy of various solutes through curdlan gels[23].

45

It is difficult to firmly state what the basis for this difference is since their comparison is scarce in literature. However, we believe that the difference in activation energy could result from the fact that the general Arrhenius model does not account for the heterogeneity exhibited by our gels while the Petit model does.
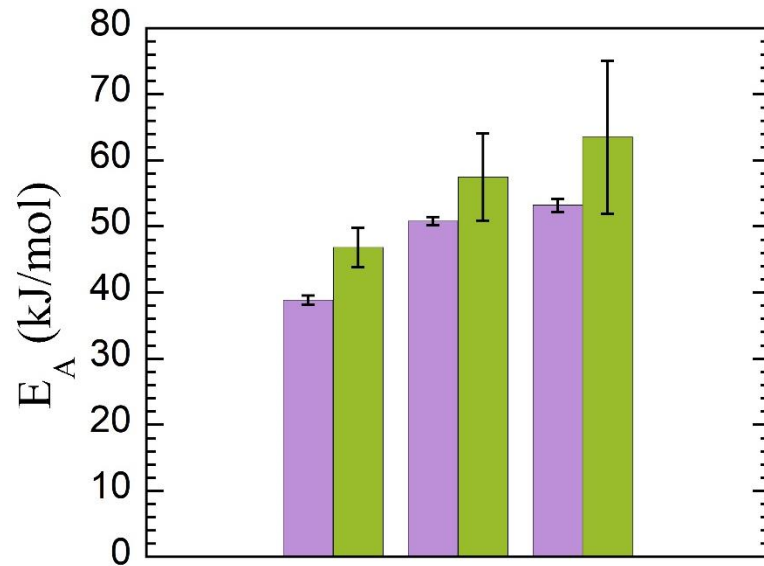
Figure 5.7: Activation energies for three types of gels. Green and purple columns represent Ea from the Petit model and the Arrhenius model, respectively.

5.2 Development of Composition-Diffusion Superposition Model

Beyond copolymer concentration, organogels can be tuned to be thermally stable at high temperature by manipulating the boiling point of the solvent used to make the gel[44]. Measurement of the diffusivity at a broad temperature range especially at high temperature, however, can be difficult because of experimental limitations. To overcome this challenge, a generalized approach to determine the diffusivity of a solute at a broad range of temperature in an organogel was investigated using our hypothetical composition-diffusion superposition model, which addresses Goal III of this research. This approach was inspired by the time-temperature superposition principle used to described polymer mechanical behavior[45]. We refer to this approach as the 'composition-diffusion superposition model' because in the development of the model we use diffusion data for gels based on oils whose composition are different (based on their identity SQ, HB200, HB380). The main idea in the composition-diffusion superposition model is that the viscosity profiles (change in viscosity with temperature) of various aliphatic oil solvents can be superimposed by taking one oil solvent profile as a reference and shifting the other profiles each by a given horizontal shift factor. The horizontal shift factors are subsequently used to combine diffusivity data collected for gels with these unique solvents into a single, master curve.

A fluid's viscosity is a measure of its resistance to flow. Viscosity is one of the most important properties of the fluids used in various industries such as chemical, pharmaceutical and cosmetic industries[46]. Additionally, viscosity impacts how fluids are designed, handled, mixed and transported[32]. It is therefore crucial to understand how different factors, primarily temperature and pressure, impact viscosity.

There are several empirical equations that relate fluid viscosity to temperature[47]. But for simplicity we choose the Arrhenius equation. Based on the Arrhenius equation, the temperature dependence of viscosity can be expressed by[48]

$$\mu = G \, exp \left(\frac{E_A}{RT} \right) \tag{5.10}$$

where μ is the viscosity, G is a constant, E_A is the flow activation energy, R is the gas constant and T is the absolute temperature. In the more common form of the Arrhenius equation, the exponential term includes a negative sign. However, Equation (5.10) has a positive exponential term because viscosity is expected to decrease with increasing temperature as opposed to other Arrhenius-type relationships, such as reaction rate constants, that are anticipated to increase with temperature[48]. Equation (5.10) can be linearized in terms of the independent and dependent variables as

$$\ln(\mu) = \ln(G) + \frac{E_A}{R} \left(\frac{1}{T} \right) \tag{5.11}$$

Therefore, plotting $\ln(\mu)$ vs. 1/T will be linear in cases of fluids with viscosities that follow the Arrhenius behavior.

Here, Arrhenius plots for different oil solvents were superimposed on a reference oil solvent to provide respective horizontal shift factors. The shift factors are then extended to description of diffusion data. Therefore, it is important to recognize how solvent viscosity impacts diffusion in gels.

In hydrodynamic models for diffusion in gels, polymer chains as well as the gel solvent cause resistance against solute diffusion[21]. So, the general expression of diffusivity of a solute in gels is

$$D_g = D_0 f(\phi) \tag{5.12}$$

where D_g is the solute diffusivity in gel, $f(\phi)$ is a function dependent on ϕ which is the volume fraction of polymer in the gel, and D_0 is the diffusivity of the probe in pure solvent. D_0 can be determined using the Stokes-Einstein equation (Equation 5.9)

$$D_0 = \frac{k_B T}{6\pi r_h \mu} \tag{5.9}$$

So, from Equation (5.12) and (5.9) it is evident that at a certain temperature for a fixed polymer gel matrix and constant solute radius, solute diffusivity in the gel depends only on the solvent viscosity. This relationship was also experimentally proven by a previous study on styrenic block copolymer organogels where the diffusivity of a solute was tuned by changing the gel solvent at ambient temperature and the diffusivity was found to be inversely related to gel solvent viscosity[10].

Along with the solvent viscosity and some other factors, solute diffusivity in a gel depends also on temperature[24]. This relationship can be explained using the general Arrhenius equation[32] (Equation 2.19)

$$D = D_{inf} \, exp\left(-\frac{E_a}{RT}\right) \tag{2.19}$$

We hypothesize that the horizontal shift factors used to construct the master curve from the viscosity profiles of different mineral oils can be used to merge temperature-dependent diffusivity data of the gels composed of these mineral oils. To test the hypothesis, at first, Arrhenius viscosity plots of Hydrobrite 380, Hydrobrite 200, Squalane were developed. Then, taking the plot of HB200 as a reference plot, the plots of the other two oils were superimposed on the reference plot by minimizing the overlap

with the reference plot using specific horizontal shift factors for HB380 and SQ plots. Then, these horizontal shift factors are applied to diffusivity values of solute through organogels consisting of copolymer poly[styrene-b-(ethylene-co-butylene)-b-styrene] (SEBS) and the same three oil solvents. Successful transformation of diffusivity values onto a master curve using the horizontal shift factors would support our hypothesis.

5.2.1 Effect of Temperature on Viscosity

To develop the composition-diffusion superposition model, our first step was to measure each oil's viscosity as a function of temperature ranging from 10 °C to 70 °C. It was observed that the viscosities of all of the oils decreased with the increase in temperature (Figure 5.8 a). This was due to the fact that the increased temperature provided the oil molecules more energy to overcome the resistance to the flow. Furthermore, each individual profile is well-described by the general Arrhenius expression displayed in Equation 5.11 (Figure 5.9 a). The R^2 values for HB380, HB200 and SQ are 0.996, 0.995, and 0.996, respectively.

(a)   (b)
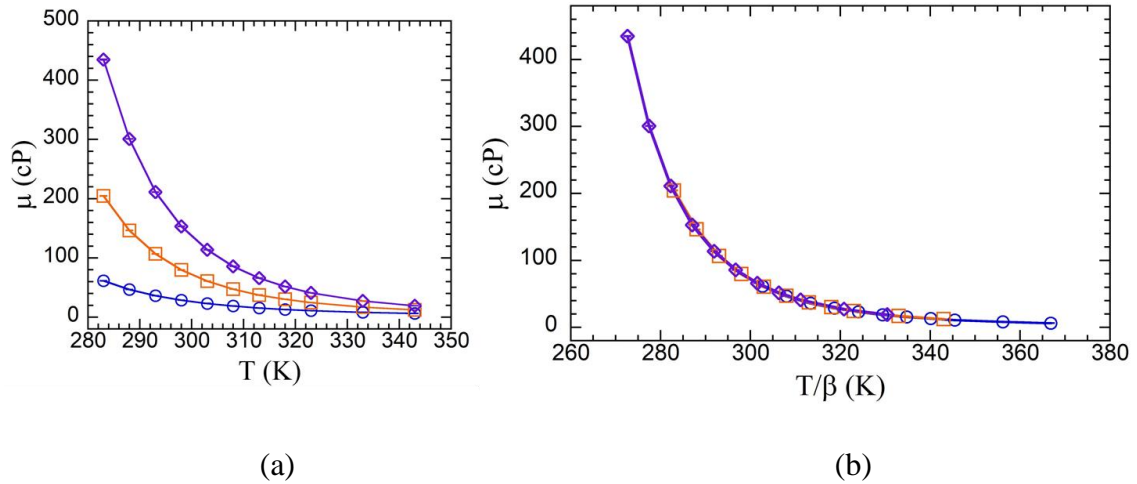
Figure 5.8:(a) Viscosity vs. temperature data for HB380 (◊), HB200 (□) and SQ (○).

(b) viscosity vs. temperature/β (combined viscosity profile incorporating the shift

factors). Solid lines are guide to the eyes.

The activation energies found from the slope E_A/R of viscosity profiles (Figure 5.9 a) for

HB380, HB200, SQ were 42.2 ± 0.7 kJ/mol, 37.8 ± 0.9 kJ/mol, 30.6 ± 0.9 kJ/mol,

respectively. Taking the viscosity profile of mineral oil HB200 as the reference, the

viscosity profiles of HB380 and SQ were superimposed by multiplying $1/T$ with

horizontal shift factors (β) to provide a combined viscosity profile ($R^2 = 0.99$) (Figure 5.9

b).

The horizontal shift factors were found by maximizing the overlap between the two

shifted viscosity profiles and the reference one. The shift factor for HB380 ($\beta1$) and SQ

($\beta2$) were found to be 1.04 and 0.94, respectively. The activation energy, E_A, for HB200

obtained from the master curve is similar to the one found from the viscosity profile of

HB200 (37.5 ± 5.1 kJ/mol).
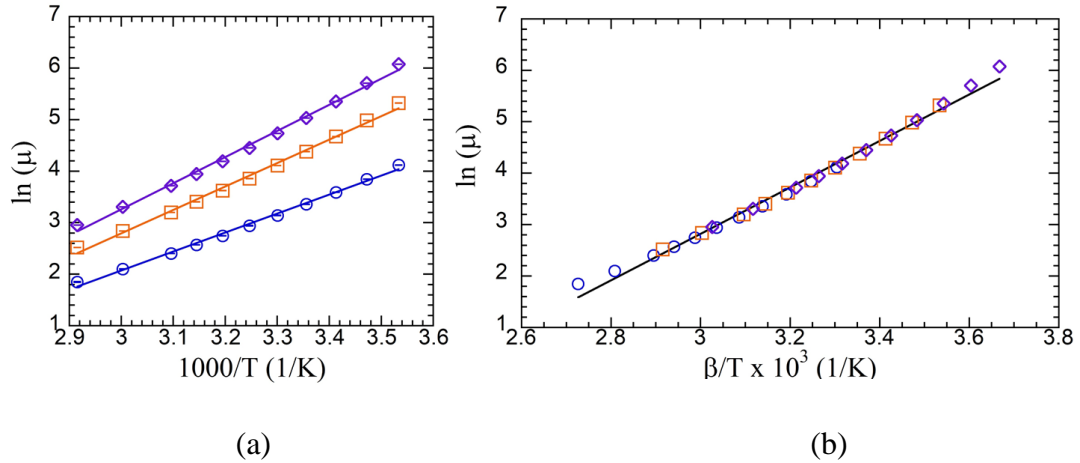
Figure 5.9: Arrhenius plots of viscosity for HB380 (◊), HB200 (□) and SQ (○) (a)

and for the superimposed viscosity profile (b). The solid lines are fit to the

Arrhenius equation.

It is shown in Figure 5.8 (a) that the experimental viscosity data for HB200 is available

within the temperature range of 283 K to 343 K. In the combined viscosity profile (Figure

5.8 b), the same shift factors as above are used. In this combined profile, data from the

higher viscosity oil (HB380) mimics viscosity data for oil HB200 at lower temperatures

(272.6 K to 282.3 K) whereas data from the lower viscosity oil (SQ) mimics viscosity

data for oil HB200 at higher temperatures (345.5 K to 366.8 K). Therefore, we could

infer that the superimposed viscosity profile (Figure 5.9 b) can be regarded as an

extended viscosity profile of oil HB200 since that was the reference condition.

5.2.2 Extension to Solute Diffusivity

With the horizontal factors in hand, we set out to investigate our hypothesis that these

shift factors can be used to superimpose temperature-dependent diffusivity data collected

from gels composed of the different mineral oils (see Section 4).

Before proceeding, however, we take some initial steps to sanity check the viscosity-dependence of our diffusivity data. As discussed above, for a system containing a fixed solute, copolymer, and copolymer concentration at a constant temperature, the solute diffusivity depends only on the viscosity of the gel solvent. Additionally, Equation 5.12 suggests that the relationship between diffusivity and inverse viscosity should be linear with the intercept equal to zero. For each formulation at a fixed temperature, we observe that diffusivity of AOT reverse micelle are, in fact, inversely related to the solvent viscosity. An example for gels at all five concentrations of SEBS at an average temperature of 25.2 °C is provided in Figure 5.10. Similar analysis of data for the other copolymer concentrations and temperatures examined are provided in Appendix A (Figure A1). Note, average temperature and composition across experiments for the three unique gels (three aliphatic oil types) are used to refer to the data set, but the experimental temperature and composition varied slightly between the different gel types.
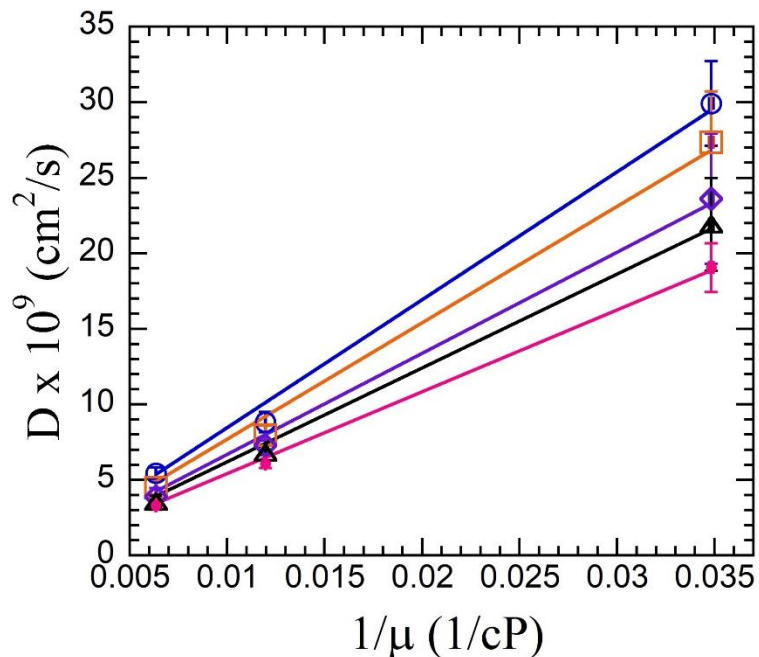
Figure 5.10: Diffusivity in gels vs. inverse viscosity of gel solvent made with average 6.7 wt% (○), 8.9 wt% (□), 11 wt% (◊), 13.3 wt% (Δ) and 14.8 wt% (●) SEBS at 25.2°C. Points from left to right refers to gels made with solvent oil HB380, HB200, SQ respectively. The line is a linear fit with a fixed intercept of zero ($R^2 \geq 0.993$ for all).

It was discussed previously that with the increase in temperature, the viscosity of the oils decreases and now it is shown above that the viscosity of the oil solvents used to make the gels impact the diffusivity of the solute through the gels. So, at various experimental temperatures, the viscosity of each oil solvent in the gel would also vary impacting the solute diffusion through the gel.

As per Equation 2.19 for a polymer gel, the plot for ln(D) vs. $1/T$ should be a straight line with the slope $-\frac{E_a}{R}$. Therefore, the diffusion activation energy can be obtained from the slope. Figure 5.11 shows the Arrhenius-type relation between the solute diffusivity and

temperature for the three types of gels with 11 wt% SEBS. The R^2 values are all ≥ 0.996

which inform that the data fits the Arrhenius-type equation well. The data for the other

gel compositions are provided in Figure 5.1.
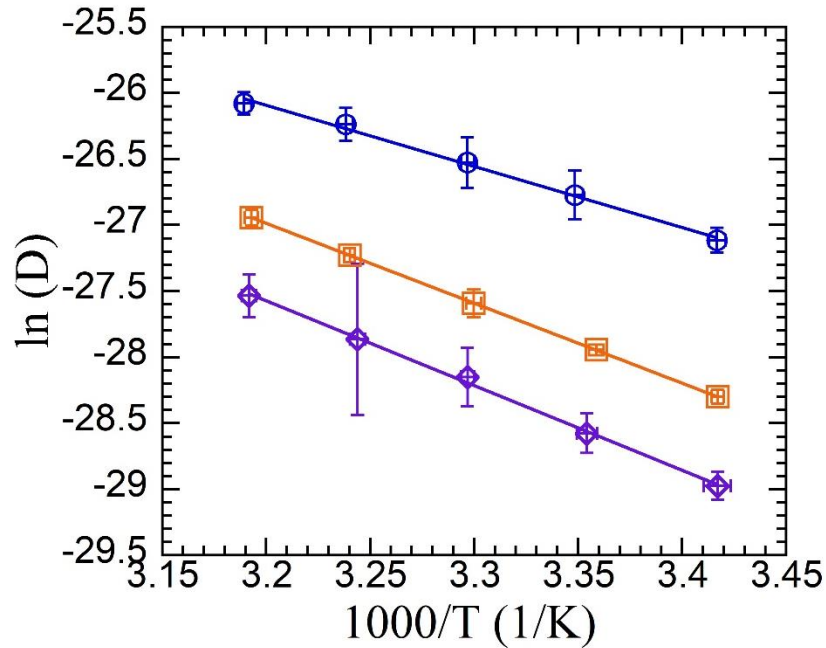
Figure 5.11: Arrhenius plot for SQ (○), HB200 (□) and HB380 (◊) for 11% SEBS.

The lines are fit to the Arrhenius equation for diffusion.

Finally, we took the temperature-dependent diffusivity data (Figure 5.11) for the gel

made with HB200 as the reference condition. The inverse temperature data (Figure 5.11)

for HB380 and SQ gels were multiplied with respective horizontal shift factors found

from the previous composition-viscosity superpositioning (1.04 and 0.94, respectively) to

obtain Figure 5.12(b). We want to emphasize that these shift factors were not determined

using diffusivity data, but rather simply applied based upon the viscosity analysis above.

(a)   (b)
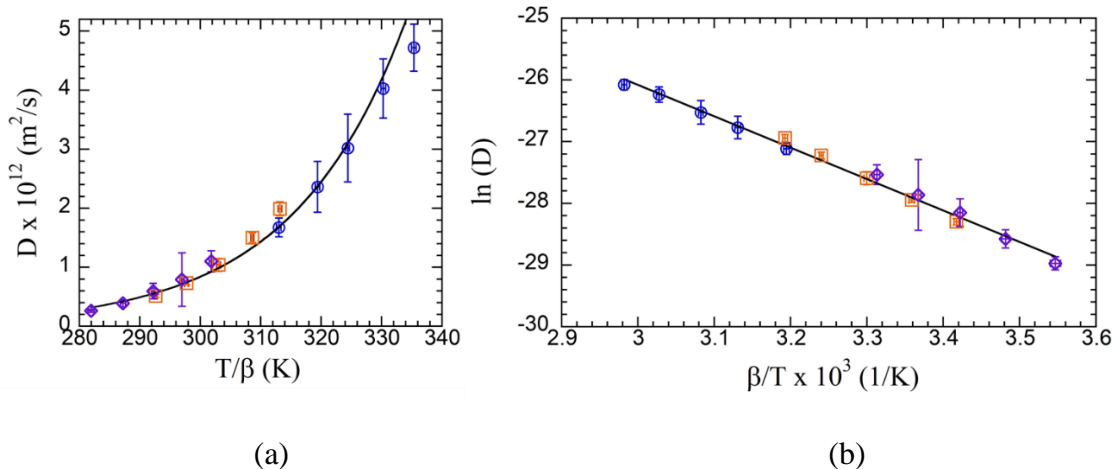
Figure 5.12: Merged data of (a) diffusivity vs. shifted temperature (solid line represents fit to Equation 2.19), (b) natural log of diffusivity vs β/temperature, for the reference gel made with 11wt% SEBS. In the plots (○), (□) and (◊) represents data from SQ, HB200 and HB380 gels. The line (b) reflects a linear fit with unified E_A value and unique D_{inf}.

Applying the shift factors results in an outstanding merge of the temperature-dependent diffusivity data of gels made with various oil solvents (Figure 5.12 a, b). The merged data for gels with other copolymer concentrations are provided in Appendix A. It is observed from Figure 5.12 (a) that before merging we had diffusivity data for HB200 within the range of ~20-40°C, and after the merge the range expanded to ~ 9-62°C. The same unified E_A fitting described and supported in Section 5.1 was used to further analyze merged data for each of the investigated gel sets. This treatment provides a good description of data here, as well (R = 0.99). The unified E_A values for the reference gels (*i.e.*, those containing HB 200) individually and from fitting merged data (Figure 5.12b) are 50.8 ± 0.6 kJ/mol and 42.3 ± 0.6 kJ/mol, respectively. We are unsure of the exact reasons for this disagreement, but speculate that it could stem from slight differences in

copolymer concentration and experimental temperature across gels with different

aliphatic oils among other things.

6. Conclusions

In this research, diffusivities of AOT reverse micelle were measured in different SEBS gels varying in gel solvent viscosity and composition at a range of temperature. The diffusivity data were analyzed using two diffusion models that account for effect of temperature on diffusion, and our data fits both of the models. The first model is a general Arrhenius model. The diffusion activation energies for gels of different concentrations were calculated using this model. We found that the activation energy is not a function of gel polymer concentration. Therefore, we determined a unified activation energy for each type of gels for a certain concentration range. The second model that we used to analyze our diffusivity data was the model of Petit *et al.* Since our gels have polystyrene crosslinks of significant size, to account for them, we incorporated Mackie and Meares obstruction model into the Petit model. Using the diffusivities, the Arrhenius model and the Petit model provided slightly different activation energies for each type of gels. For SEBS+SQ, SEBS+HB200 and SEBS+HB380 gels the activation energies found from the Arrhenius model were 38.9 ± 0.7, 50.8 ± 0.6, 53.2 ± 1 kJ/mol and from the Petit model were 46.8 ± 3, 57.5 ± 6.6 and 63.5 ± 11.6 kJ/mol, respectively. In this research, we also developed a composition-diffusion superposition model using three oil solvents having different viscosities. Taking one oil solvent as a reference, two horizontal shift factors were obtained for the other two oils. Using the shift factors, solute diffusivity in gels made with the reference oil solvent could be estimated at a broader temperature range.

7. Future Work

It was an initial plan for our project to also include the analysis on the impact of polymer molecular weight on the diffusion activation energy of AOT reverse micelle. In order to do that we ran the experiments on two other types of polymer gels having varying molecular weight. Since the experimental setup was newly built just for this project, we faced some unexpected challenges such as maintaining the set temperature in the sample enclosures, electrical issues, and problems with the thermocouple probe that we needed to troubleshoot. As a result, the experiments done early on, including for those molecular weights, are not at a sufficiently trustworthy level to be formally presented. Repeating experiments for one type of polymer requires about two months. Due to lack of time, this part of the project lacks concrete conclusions. It would still be interesting to explore this part in the future and determine the impact of polymer molecular weight on diffusion activation energy.

As presented in previous chapters, we investigated the impact of gel solvent viscosity on the activation energy. There are several other factors that impact activation energy among which solute size would be an important factor to investigate as it would inform the diffusion behavior of different size drugs in gels made with SEBS and mineral oil. Currently, there are several solutes such as Span 80, Span 85, oleic acid and poly (hydroxystearic acid) (Figure 7.1) that vary in molecular size and are compatible with our gel systems. Investigating temperature dependent diffusion of these in our gels would provide information about the impact of solute size on the diffusion activation energy.
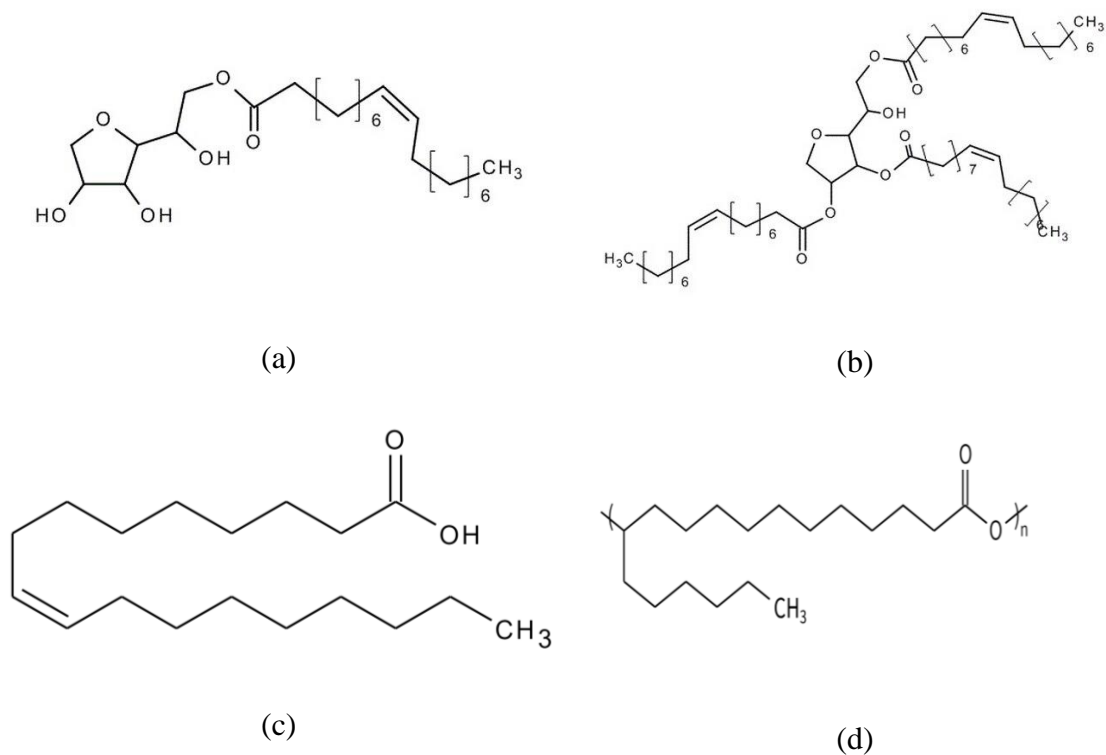
Figure 7.1: (a) Span 80, (b) Span 85, (c) oleic acid and (d) poly (hydroxystearic acid)

Finally, there are several future research directions that can be explored regarding the composition-diffusion superposition model. One of them would be to expand the master curve by using oils of lower (*e.g.*, dodecane) and higher viscosity (*e.g.*, HB550) than the ones we used and check the model's validity to predict diffusivity at a broader temperature range. Alternatively, a similar analysis could be completed using a different solute like those discussed in the previous paragraph.

8. References

(1) Mineart, K. P.; Walker, W. W.; Mogollon-Santiana, J.; Lee, B. A Fourier Transform Infrared Spectroscopy- BASED Method for Tracking Diffusion in Organogels. *Journal of Polymer Science* **2020**, *58* (12), 1707–1716. https://doi.org/10.1002/pol.20200144.

(2) Esposito, C. L.; Kirilov, P.; Roullin, V. G. Organogels, Promising Drug Delivery Systems: An Update of State-of-the-Art and Recent Applications. *Journal of Controlled Release* **2018**, *271*, 1–20. https://doi.org/10.1016/j.jconrel.2017.12.019.

(3) Prausnitz, M. R.; Langer, R. Transdermal Drug Delivery. *Nat Biotechnol* **2008**, *26* (11), 1261–1268. https://doi.org/10.1038/nbt.1504.

(4) Alkilani, A.; McCrudden, M. T.; Donnelly, R. Transdermal Drug Delivery: Innovative Pharmaceutical Developments Based on Disruption of the Barrier Properties of the Stratum Corneum. *Pharmaceutics* **2015**, *7* (4), 438–470. https://doi.org/10.3390/pharmaceutics7040438.

(5) Ma, J.; Wang, C.; Luo, H.; Zhu, Z.; Wu, Y.; Wang, H. Design and Evaluation of a Monolithic Drug-in-Adhesive Patch for Testosterone Based on Styrene–Isoprene–Styrene Block Copolymer. *Journal of Pharmaceutical Sciences* **2013**, *102* (7), 2221–2234. https://doi.org/10.1002/jps.23576.

(6) *Transdermal Components– Delivering More than Just Medicine Https://Multimedia.3m.Com/Mws/Media/1153325O/3m-Transdermal-Components-e-Book.Pdf*.

(7) Gennari, C. G. M.; Quaroni, G. M. G.; Creton, C.; Minghetti, P.; Cilurzo, F. SEBS Block Copolymers as Novel Materials to Design Transdermal Patches. *International*

Journal of Pharmaceutics **2020**, *575*, 118975.
https://doi.org/10.1016/j.ijpharm.2019.118975.

(8)   Walker, William, "Dual Self-Assembly of a Selectively Solvated ABA Triblock
       Copolymer Network Loaded with Reverse Micelles" (2019). Master's Theses. 216.
       Https://Digitalcommons.Bucknell.Edu/Masters_theses/216.

(9)   Mineart, K. P.; Walker, W. W.; Mogollon-Santiana, J.; Coates, I. A.; Hong, C.; Lee,
       B. Nanocarrier-Loaded Block Copolymer Dual Domain Organogels. *Polymer* **2021**,
       214, 123246. https://doi.org/10.1016/j.polymer.2020.123246.

(10)   Mineart, K. P.; Hong, C.; Rankin, L. A. Decoupling of Mechanical and Transport
       Properties in Organogels via Solvent Variation. *Gels* **2021**, *7* (2), 61.
       https://doi.org/10.3390/gels7020061.

(11)   Rankin, L. A.; Lee, B.; Mineart, K. P. Effect of Network Connectivity on the
       Mechanical and Transport Properties of Block Copolymer Gels. *Journal of Polymer
       Science* **2021**, *59* (1), 34–42. https://doi.org/10.1002/pol.20200695.

(12)   Matsen, M. W.; Schick, M. Self-Assembly of Block Copolymers. *Current Opinion
       in Colloid & Interface Science* **1996**, *1* (3), 329–336. https://doi.org/10.1016/S1359-
       0294(96)80128-2.

(13)   Hamley, I. W. *The Physics of Block Copolymers Oxford Univ*; Press, 1998.

(14)   Borsali, R.; Pecora, R. *Soft-Matter Characterization*; Springer Science & Business
       Media, 2008.

(15)   Leibler, L. Theory of Microphase Separation in Block Copolymers.
       Macromolecules **1980**, *13* (6), 1602–1617. https://doi.org/10.1021/ma60078a047.

(16) Bates, F. S.; Fredrickson, G. H. Block Copolymers—Designer Soft Materials. *Physics Today* **1999**, *52* (2), 32–38. https://doi.org/10.1063/1.882522.

(17) Matsen, M. W.; Thompson, R. B. Equilibrium Behavior of Symmetric ABA Triblock Copolymer Melts. *The Journal of Chemical Physics* **1999**, *111* (15), 7139–7146. https://doi.org/10.1063/1.480006.

(18) Tan, H.; Watanabe, H.; Matsumiya, Y.; Kanaya, T.; Takahashi, Y. Shear-Induced Disruption and Recovery of Microphase-Separated Network Structure of a BSB Triblock Copolymer in Dibutyl Phthalate. *Macromolecules* **2003**, *36* (8), 2886–2893. https://doi.org/10.1021/ma021654q.

(19) Laurer, J. H.; Khan, S. A.; Spontak, R. J.; Satkowski, M. M.; Grothaus, J. T.; Smith, S. D.; Lin, J. S. Morphology and Rheology of SIS and SEPS Triblock Copolymers in the Presence of a Midblock-Selective Solvent. *Langmuir* **1999**, *15* (23), 7947–7955. https://doi.org/10.1021/la981441n.

(20) Vega, D. A.; Sebastian, J. M.; Loo, Y.-L.; Register, R. A. Phase Behavior and Viscoelastic Properties of Entangled Block Copolymer Gels. *J. Polym. Sci. B Polym. Phys.* **2001**, *39* (18), 2183–2197. https://doi.org/10.1002/polb.1192.

(21) Amsden, B. Solute Diffusion within Hydrogels. Mechanisms and Models. *Macromolecules* **1998**, *31* (23), 8382–8395. https://doi.org/10.1021/ma980765f.

(22) Baille, W. E.; Zhu, X. X.; Fomine, S. Study of Self-Diffusion of Hyperbranched Polyglycidols in Poly(Vinyl Alcohol) Solutions and Gels by Pulsed-Field Gradient NMR Spectroscopy. *Macromolecules* **2004**, *37* (23), 8569–8576. https://doi.org/10.1021/ma049588a.

(23) Kwak, S.; Lafleur, M. Self-Diffusion of Macromolecules and Macroassemblies in Curdlan Gels as Examined by PFG-SE NMR Technique. *Colloids and Surfaces A: Physicochemical and Engineering Aspects* **2003**, *221* (1–3), 231–242. https://doi.org/10.1016/S0927-7757(03)00145-6.

(24) Muhr, A. H.; Blanshard, J. M. V. Diffusion in Gels. *Polymer* **1982**, *23* (7), 1012–1026. https://doi.org/10.1016/0032-3861(82)90402-5.

(25) Sebti, I.; Blanc, D.; Carnet-Ripoche, A.; Saurel, R.; Coma, V. Experimental Study and Modeling of Nisin Diffusion in Agarose Gels. *Journal of Food Engineering* **2004**, *63* (2), 185–190. https://doi.org/10.1016/S0260-8774(03)00299-1.

(26) Malmsten, M.; Lindman, B. Water Self-Diffusion in Aqueous Block Copolymer Solutions. *Macromolecules* **1992**, *25* (20), 5446–5450. https://doi.org/10.1021/ma00046a050.

(27) Masaro, L.; Zhu, X. X.; Macdonald, P. M. Self-Diffusion of Oligo- and Poly(Ethylene Glycol)s in Poly(Vinyl Alcohol) Aqueous Solutions As Studied by Pulsed-Gradient NMR Spectroscopy. *Macromolecules* **1998**, *31* (12), 3880–3885. https://doi.org/10.1021/ma9710242.

(28) Øyaas, J.; Storrø, I.; Svendsen, H.; Levine, D. W. The Effective Diffusion Coefficient and the Distribution Constant for Small Molecules in Calcium-Alginate Gel Beads: EFFECTIVE DIFFUSION IN C A -ALGINATE GEL BEADS. *Biotechnol. Bioeng.* **1995**, *47* (4), 492–500. https://doi.org/10.1002/bit.260470411.

(29) Giannakopoulos, A.; Guilbert, S. Determination of Sorbic Acid Diffusivity in Model Food Gels. *International Journal of Food Science & Technology* **2007**, *21* (3), 339–353. https://doi.org/10.1111/j.1365-2621.1986.tb00413.x.

(30) Hendrickx, M.; Abeele, C. V.; Engels, C.; Tobback, P. Diffusion of Glucose in Carrageenan Gels. *J Food Science* **1986**, *51* (6), 1544–1546. https://doi.org/10.1111/j.1365-2621.1986.tb13855.x.

(31) Masaro, L.; Zhu, X. X. Physical Models of Diffusion for Polymer Solutions, Gels and Solids. *Progress in Polymer Science* **1999**, *24* (5), 731–775. https://doi.org/10.1016/S0079-6700(99)00016-7.

(32) Messaâdi, A.; Dhouibi, N.; Hamda, H.; Belgacem, F. B. M.; Adbelkader, Y. H.; Ouerfelli, N.; Hamzaoui, A. H. A New Equation Relating the Viscosity Arrhenius Temperature and the Activation Energy for Some Newtonian Classical Solvents. *Journal of Chemistry* **2015**, *2015*, 1–12. https://doi.org/10.1155/2015/163262.

(33) Petit, J.-M.; Roux, B.; Zhu, X. X.; Macdonald, P. M. A New Physical Model for the Diffusion of Solvents and Solute Probes in Polymer Solutions. *Macromolecules* **1996**, *29* (18), 6031–6036. https://doi.org/10.1021/ma951159c.

(34) Macey RI. In: Andreoli TE, Hoffman JF, Fanestil DD, Editors. Membrane Physiology. New York: Plenum Press,1980. p. 125[Chapter7].

(35) Kramers, H. A. Brownian Motion in a Field of Force and the Diffusion Model of Chemical Reactions. *Physica* **1940**, *7* (4), 284–304. https://doi.org/10.1016/S0031-8914(40)90098-2.

(36) De Gennes, P.-G.; Gennes, P.-G. *Scaling Concepts in Polymer Physics*; Cornell university press, 1979.

(37) Golden, K.; Goldstein, S.; Lebowitz, J. L. Classical Transport in Modulated Structures. *Phys. Rev. Lett.* **1985**, *55* (24), 2629–2632. https://doi.org/10.1103/PhysRevLett.55.2629.

(38) Zwanzig, R. Diffusion in a Rough Potential. *Proc. Natl. Acad. Sci. U.S.A.* **1988**, *85* (7), 2029–2030. https://doi.org/10.1073/pnas.85.7.2029.

(39) Lee, L. S. Creep and Time-Dependent Response of Composites. In *Durability of Composites for Civil Structural Applications*; Elsevier, 2007; pp 150–169. https://doi.org/10.1533/9781845693565.1.150.

(40) Mineart, K. P.; Vallely, M. J.; O'Shea, E. K. Nanostructure Scaling in Semi-Dilute Triblock Copolymer Gels. *Macro Chemistry & Physics* **2023**, 2300093. https://doi.org/10.1002/macp.202300093.

(41) The Diffusion of Electrolytes in a Cation-Exchange Resin Membrane I. Theoretical. *Proc. R. Soc. Lond. A* **1955**, *232* (1191), 498–509. https://doi.org/10.1098/rspa.1955.0234.

(42) Zhang, S.; Lee, K. H.; Sun, J.; Frisbie, C. D.; Lodge, T. P. Viscoelastic Properties, Ionic Conductivity, and Materials Design Considerations for Poly(Styrene- *b* - Ethylene Oxide- *b* -Styrene)-Based Ion Gel Electrolytes. *Macromolecules* **2011**, *44* (22), 8981–8989. https://doi.org/10.1021/ma201356j.

(43) Karvar, M.; Strubbe, F.; Beunis, F.; Kemp, R.; Smith, N.; Goulding, M.; Neyts, K. Investigation of Various Types of Inverse Micelles in Nonpolar Liquids Using Transient Current Measurements. *Langmuir* **2014**, *30* (41), 12138–12143. https://doi.org/10.1021/la502287m.

(44) Kuzina, M. A.; Kartsev, D. D.; Stratonovich, A. V.; Levkin, P. A. Organogels versus Hydrogels: Advantages, Challenges, and Applications. *Adv Funct Materials* **2023**, 2301421. https://doi.org/10.1002/adfm.202301421.

(45) Ferry, J. D. *Viscoelastic Properties of Polymers*; John Wiley & Sons, 1980.

(46) Herráez, J. V.; Belda, R.; Díez, O.; Herráez, M. An Equation for the Correlation of Viscosities of Binary Mixtures. *J Solution Chem* **2008**, *37* (2), 233–248. https://doi.org/10.1007/s10953-007-9226-2.

(47) Haj-Kacem, R. B.; Ouerfelli, N.; Herráez, J. V.; Guettari, M.; Hamda, H.; Dallel, M. Contribution to Modeling the Viscosity Arrhenius-Type Equation for Some Solvents by Statistical Correlations Analysis. *Fluid Phase Equilibria* **2014**, *383*, 11–20. https://doi.org/10.1016/j.fluid.2014.09.023.

(48) Budtova, T.; Navard, P. Viscosity-Temperature Dependence and Activation Energy of Cellulose Solutions. *Nordic Pulp & Paper Research Journal* **2015**, *30* (1), 99–104. https://doi.org/10.3183/npprj-2015-30-01-p099-104.

Appendix A

Mesh size calculations

In our SEBS gels, mesh size represents the distance between the EB polymer chains in the EB/oil matrix. Gel mesh size, ξ was calculated using

$$\xi = R_g \left(\frac{c^*}{c_{EB}}\right)^\nu$$

where R_g is radius of gyration of the polymer, c^* is the overlap concentration, c_{EB} is the concentration of EB in EB/oil matrix, and ν (= 0.588) is a constant for a given system.

R_g is calculated by

$$R_g = \sqrt{\frac{c_\propto n l^2}{6}} = 12.7 \ nm$$

where $c_\propto$ is the characteristic Flory ratio (6.42 for EB blocks), l is the segment length which is the distance between the carbon-carbon single bond (0.154 nm) and n is the number of segments in the EB block. n is calculated by

$$n = 2 \left(MW \ (1 - f_s)\right) \left(\frac{f_{EB,E}}{PE} + \frac{f_{EB,B}}{PB}\right)$$

where MW is the molecular weight of SEBS (= 157500 g/mol), f_s (= 0.278) is the mass fraction of polystyrene in SEBS, $f_{EB,E}$ (= 0.568) and $f_{EB,B}$ (= 0.432) are the mass fractions of polyethylene and polybutylene in EB, respectively and PE (= 28.04 g/mol) and PB (= 56.12 g/mol) are the repeat unit masses of polyethylene and polybutylene, respectively.

c^* is calculated by

$$c^* = \frac{M_{EB}}{\frac{4}{3}\pi R_g^3} = 0.022 \text{ g/cm}^3$$

where M_{EB} is the molecular weight of EB block. The process to calculate $c = c_{EB}$ was

shown in section 5.2.

Table A1: D_{inf}, E_A and R^2 values from Figure 5.1, and unified E_A and subsequent D_{inf}.

Gels	Polymer (wt%)	$D_{inf} \times 10^4$ (m²/s)	E_A (kJ/mol)	R^2	Unified E_A (kJ/mol)	$D_{inf} \times 10^4$ from unified E_A (m²/s)
SEBS +380	6.8 ± 0.01	8.04 ± 2	52.5 ± 3.7	0.985	53.2 ± 1.0	10.7 ± 1.5
	8.8 ± 0.03	3.46 ± 0.7	50.1 ± 2.9	0.990		9.1 ± 1.2
	10.9 ± 0.05	8.51 ± 2.2	53.3 ± 1.5	0.998		8.3 ± 2.0
	13.2 ± 0.03	24.4 ± 3.1	56.2 ± 1.1	0.999		7.5 ± 0.8
	15.3 ± 0.09	7.21 ± 1.2	53.3 ± 1.2	0.999		6.9 ± 1.0
SEBS +200	6.2 ± 0.00	2.77 ± 0.3	48.4 ± 0.5	1	50.8 ± 0.6	7.0 ± 0.8
	8.4 ± 0.00	11.5 ± 0.16	52.2 ± 1.4	0.998		6.6 ± 0.7
	10.5 ± 0.01	4.86 ± 0.3	50.3 ± 0.2	1		5.9 ± 0.4
	12.7 ± 0.04	5.90 ± 0.6	51.0 ± 0.5	1		5.5 ± 0.5
	14.5 ± 0.01	7.81 ± 1.0	52.1 ± 2.6	0.993		4.7 ± 0.9
SEBS +SQ	7.1 ± 0.02	0.13 ± 0.01	38.0 ± 1.2	0.997	38.9 ± 0.7	0.18 ± 0.02
	9.4 ± 0.1	0.09 ± 0.01	37.3 ± 1.3	0.996		0.16 ± 0.02
	11.7 ± 0.02	0.13 ± 0.02	38.5 ± 1.5	0.996		0.15 ± 0.02
	14.0 ± 0.04	0.28 ± 0.05	40.7 ± 2.4	0.990		0.13 ± 0.02
	16.3 ± 0.00	0.17 ± 0.02	39.7 ± 1.1	0.998		0.12 ± 0.01
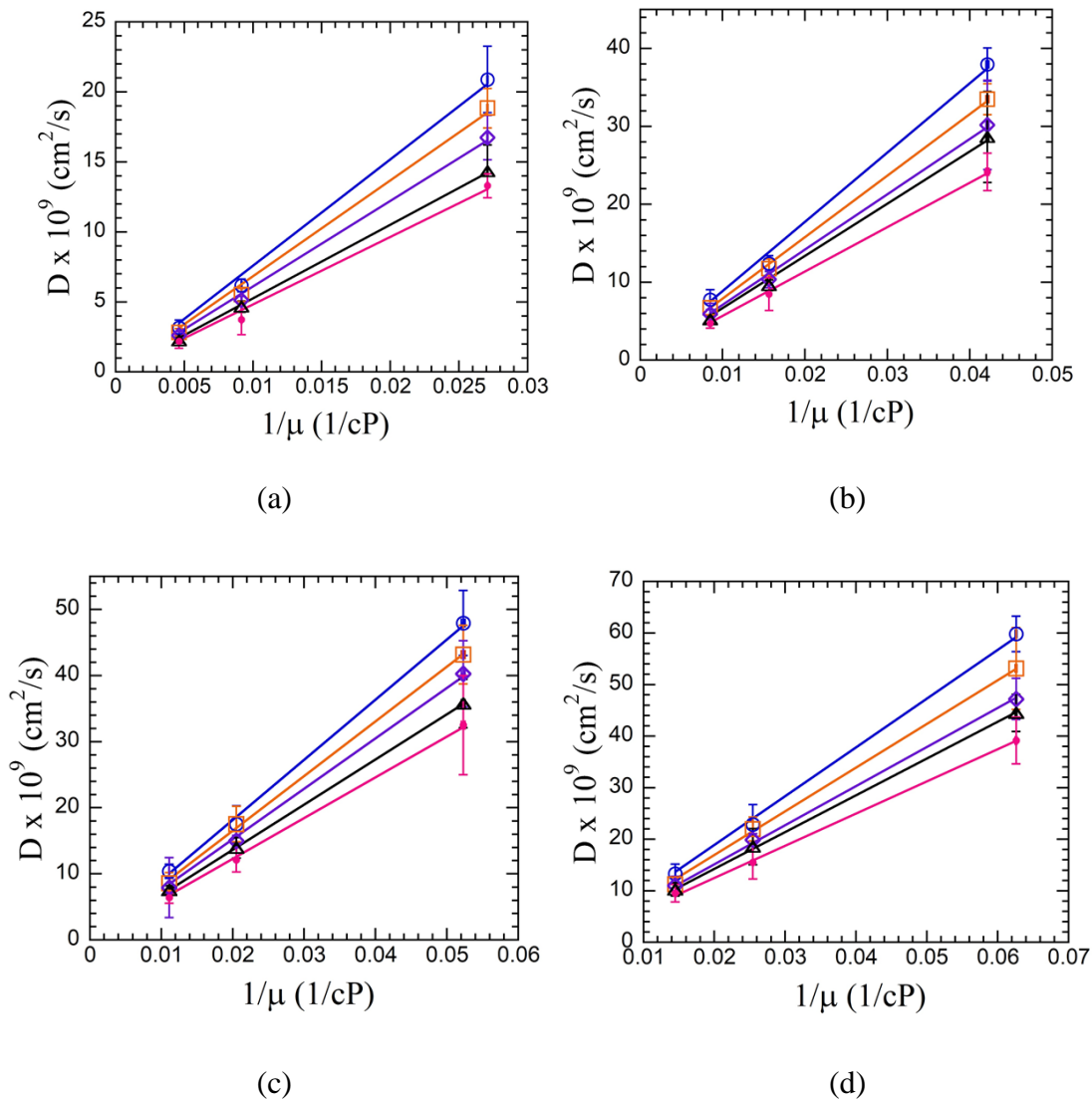
Figure A1: Diffusivity in gels vs. inverse viscosity of gel solvent made with average 6.7 wt% (○), 8.9 wt% (□), 11 wt% (◇), 13.3 wt% (Δ) and 14.8 wt% (●) SEBS at (a) 19.7°C, (b) 30.2°C (c) 35.6 °C and (d) 40.3 °C. Points from left to right refers to gels made with solvent oil HB380, HB200, SQ respectively. The line is a linear fit with a fixed intercept of zero ($R^2 \geq 0.993$ for all).

Figure A2: Natural log of diffusivity vs β/temperature, for the reference gel made with 6.7 wt% (a), 8.9 wt% (b), 13.3 wt% (c) and 14.8 wt% (d) SEBS. In the plots (○), (□) and (◊) represents data from SQ, HB200 and HB380 gels. R^2 values for all are ≥ 0.99. The solid line reflects a linear fit with unified Ea value and unique D_{inf}.

Appendix B

Uncertainty Calculations

ΔD :

Diffusivity is determined from FTIR experiments using

$$\frac{m}{m_0} = \sum_{n=1}^{\infty} \frac{8}{(2n-1)^2 \pi^2} \exp\left(\frac{-D\pi^2(2n-1)^2}{4L^2}t\right)$$
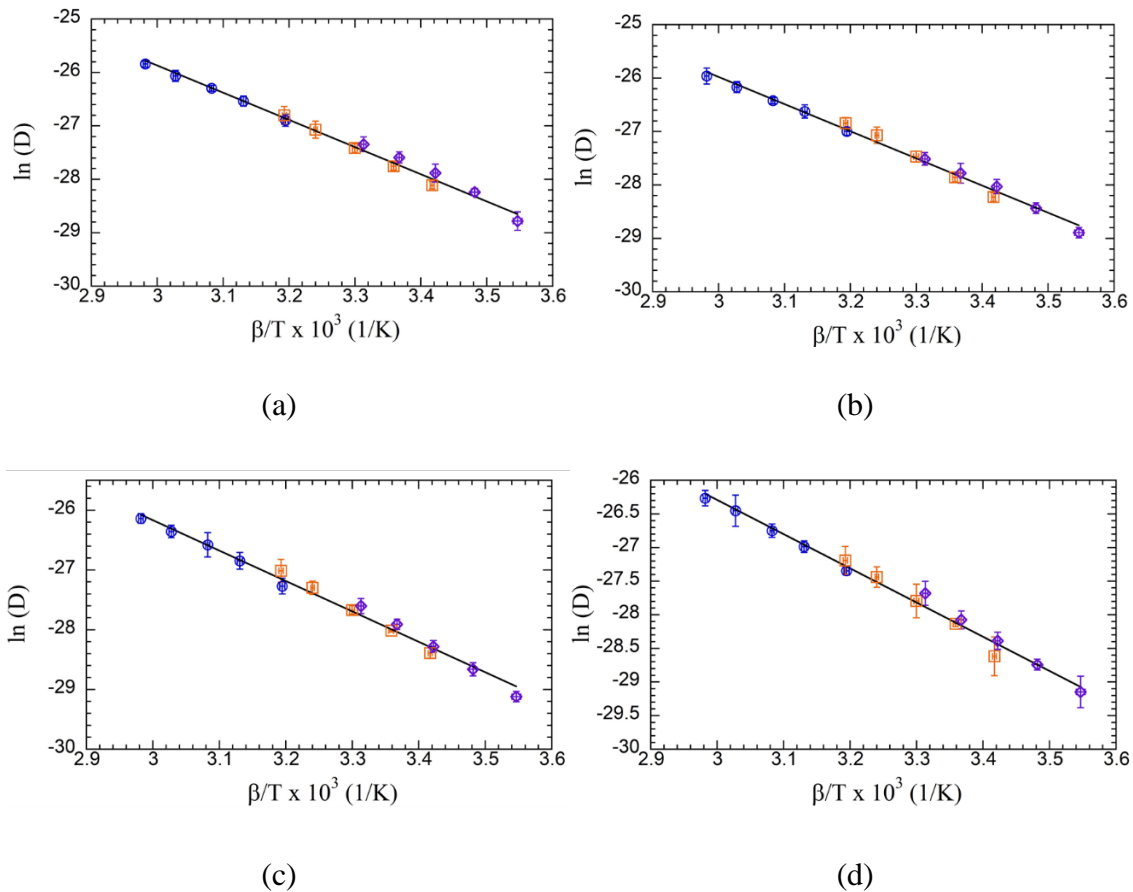
Solving algebraically for D (using first-term as an approximation):

$$D = -\left(\frac{4L^2}{\pi^2 t}\right) \ln\left\{\left(\frac{\pi^2}{8}\right)\left(\frac{m}{m_0}\right)\right\}$$

The variables (m/m_0) and L (half-thickness) are the only terms with significant uncertainty:

$$\Delta D = \sqrt{\left[\left|\frac{\delta D}{\delta\left(\frac{m}{m_0}\right)}\right| \Delta\left(\frac{m}{m_0}\right)\right]^2 + \left[\left|\frac{\delta D}{\delta L}\right| \Delta L\right]^2}$$

$$\Delta D = \sqrt{\left[\left(\frac{4L^2}{\left(\frac{m}{m_0}\right)\pi^2 t}\right) \Delta\left(\frac{m}{m_0}\right)\right]^2 + \left[\left(\frac{8L}{\pi^2 t}\ln\left(\left(\frac{\pi^2}{8}\right)\left(\frac{m}{m_0}\right)\right)\right)\Delta L\right]^2}$$

$$\Delta D = \sqrt{\left[(D)\frac{\Delta\left(\frac{m}{m_0}\right)}{\left(\frac{m}{m_0}\right)\ln\left\{\left(\frac{\pi^2}{8}\right)\left(\frac{m}{m_0}\right)\right\}}\right]^2 + \left[(2D)\frac{\Delta L}{L}\right]^2}$$

*Average values of $\Delta(m/m_0)/|(m/m_0)\ln\{(\pi^2/8)(m/m_0)|$ and $\Delta L/L$ were used

Δln (D):

$$\Delta(\ln D) = \sqrt{\left[\left|\frac{\delta(\ln D)}{\delta D}\right|\Delta D\right]^2} = \left|\frac{\delta(\ln D)}{\delta D}\right|\Delta D = \left(\frac{1}{D}\right)\Delta D = \frac{\Delta D}{D}$$

Δ(1/T):

$$\Delta\left(\frac{1}{T}\right) = \sqrt{\left[\left|\frac{\delta\left(\frac{1}{T}\right)}{\delta T}\right|\Delta T\right]^2} = \left|\frac{\delta\left(\frac{1}{T}\right)}{\delta T}\right|\Delta T = \left(\frac{1}{T^2}\right)\Delta T = \left(\frac{1}{T}\right)\frac{\Delta T}{T}$$

ΔE$_A$ (for General Arrhenius Model):

Activation energy is determined by fitting D vs T using

$$D = D_{inf}e^{-E_A/RT}$$

Algebraically rearranging to solve for E_A gives

$$E_A = -RT \ln\left(\frac{D}{D_{inf}}\right)$$

The uncertainty stems from D and T therefore

$$\Delta E_A = \sqrt{\left[\left|\frac{\delta E_A}{\delta T}\right|\Delta T\right]^2 + \left[\left|\frac{\delta E_A}{\delta D}\right|\Delta D\right]^2 + \left[E_A\frac{\Delta\left(\frac{E_A}{R}\right)}{\left(\frac{E_A}{R}\right)}\right]^2}$$

$$\Delta E_A = \sqrt{\left[\left(-R \ln\left(\frac{k}{D_{inf}}\right)\right)\Delta T\right]^2 + \left[\left(\frac{RT}{D}\right)\Delta D\right]^2 + \left[E_A\frac{\Delta\left(\frac{E_A}{R}\right)}{\left(\frac{E_A}{R}\right)}\right]^2}$$

$$\Delta E_A = \sqrt{\left[E_A \frac{\Delta T}{T}\right]^2 + \left[E_A \frac{\Delta D}{D \ln(D/D_{inf})}\right]^2 + \left[E_A \frac{\Delta\left(\frac{E_A}{R}\right)}{\left(\frac{E_A}{R}\right)}\right]^2}$$

*Average values of $\Delta T/T$ and $\Delta D/|D\ln(D/D_{inf})|$ were used and $\Delta(E_A/R)/(E_A/R)$ comes from fitting of slope ($\ln D$ vs. $1/T$)

ΔD_{inf}:

General Arrhenius model is stated as

$$D = D_{inf}e^{-E_A/RT}$$

Algebraically rearranging to solve for D_{inf} gives

$$D_{inf} = \frac{D}{e^{-\frac{E_A}{RT}}}$$

The uncertainty stems from D and $1/T$ therefore

$$\Delta D_{inf} = \sqrt{\left[\left|\frac{\delta D_{inf}}{\delta\left(\frac{1}{T}\right)}\right|\Delta(\tfrac{1}{T})\right]^2 + \left[\left|\frac{\delta D_{inf}}{\delta D}\right|\Delta D\right]^2 + \left[D_{inf}\frac{\Delta(\ln D_{inf})}{(\ln D_{inf})}\right]^2}$$

$$\Delta D_{inf} = \sqrt{\left[\left(\frac{E_A}{R}\left(De^{\frac{E_A}{RT}}\right)\right)\Delta(\tfrac{1}{T})\right]^2 + \left[\left(e^{\frac{E_A}{RT}}\right)\Delta D\right]^2 + \left[D_{inf}\frac{\Delta(\ln D_{inf})}{(\ln D_{inf})}\right]^2}$$

$$\Delta D_{inf} = \sqrt{\left[\left(D_{inf}\frac{E_A}{R}\right)\Delta(\tfrac{1}{T})\right]^2 + \left[D_{inf}\left(\frac{\Delta D}{D}\right)\right]^2 + \left[D_{inf}\frac{\Delta(\ln D_{inf})}{(\ln D_{inf})}\right]^2}$$

*Average value of $\Delta D/D$ was used and $\frac{\Delta(\ln D_{inf})}{(\ln D_{inf})}$ comes from fitting of intercept of ($\ln D$ vs. $1/T$).

Δc_{EB}:

The measured variable w_{SEBS} (concentration of SEBS triblock copolymer in a gel) is used

to determine c_{EB} (the concentration of midblocks within the midblock/oil matrix) via

$$c_{EB} = \frac{w_{SEBS}(1 - f_s)\rho_{EB/MO}}{1 - w_{SEBS}f_s}$$

The only significant source of uncertainty is w_{SEBS}. Therefore, uncertainty in c_{EB} is

determined by

$$\Delta c_{EB} = \sqrt{\left[\left|\frac{\delta c_{EB}}{\delta w_{SEBS}}\right| \Delta w_{SEBS}\right]^2} = \left|\frac{\delta c_{EB}}{\delta w_{SEBS}}\right| \Delta w_{SEBS} = \left|\frac{(f_s - 1)\rho_{EB/MO}}{(1 - f_s w_{SEBS})^2}\right| \Delta w_{SEBS}$$

$$\Delta c_{EB} = c_{EB} \frac{\Delta w_{SEBS}}{w_{SEBS}(1 - f_s w_{SEBS})}$$

Uncertainty from c_{EB} must be propagated to ξ and $1/\xi^2$. (The only significant uncertainty

here is from c_{EB}.)

Definitions of each term

$$\xi = R_g \left(\frac{c_{EB}^*}{c_{EB}}\right)^{\nu} \qquad \frac{1}{\xi^2} = \frac{1}{R_g^2}\left(\frac{c_{EB}}{c_{EB}^*}\right)^{2\nu}$$

Finding uncertainties

$$\Delta\xi = \sqrt{\left[\left|\frac{\delta\xi}{\delta c_{EB}}\right| \Delta c_{EB}\right]^2} = \left|\frac{\delta\xi}{\delta c_{EB}}\right| \Delta c_{EB} = \left(\frac{\nu R_g (c_{EB}^*/c_{EB})^{\nu}}{c_{EB}}\right) \Delta c_{EB} = \nu\xi \frac{\Delta c_{EB}}{c_{EB}}$$

$\Delta\left(\frac{1}{\xi^2}\right):$

$$\Delta\left(\frac{1}{\xi^2}\right) = \sqrt{\left[\left|\frac{\delta\left(\frac{1}{\xi^2}\right)}{\delta c_{EB}}\right|\Delta c_{EB}\right]^2} = \left|\frac{\delta\left(\frac{1}{\xi^2}\right)}{\delta c_{EB}}\right|\Delta c_{EB} = \left(\frac{2\nu(c_{EB}/c_{EB}^*)^{2\nu}}{c_B R_g^{\,2}}\right)\Delta c_{EB}$$

$$= 2\nu\left(\frac{1}{\xi^2}\right)\frac{\Delta c_{EB}}{c_{EB}}$$

ΔD_0 and Δk :

The Petit model equation for fitting diffusivity data is

$$\frac{1}{D} = \left(\frac{1+\phi_A}{1-\phi_A}\right)^2\left(\frac{1}{D_0} + \frac{1}{k\xi^2}\right)$$

Solving for the two fitted terms

$$D_0 = \frac{1}{\left(\frac{1-\phi_A}{1+\phi_A}\right)^2\frac{1}{D} - \frac{1}{k\xi^2}} \qquad\qquad k = \left(\frac{1}{\xi^2}\right)\frac{1}{\left(\frac{1-\phi_A}{1+\phi_A}\right)^2\frac{1}{D} - \frac{1}{D_0}}$$

Uncertainty stems from $1/D$ and $1/\xi^2$ therefore

$$\Delta D_0 = \sqrt{\left[\left|\frac{\delta D_0}{\delta\left(\frac{1}{D}\right)}\right|\Delta\left(\frac{1}{D}\right)\right]^2 + \left[\left|\frac{\delta D_0}{\delta\left(\frac{1}{\xi^2}\right)}\right|\Delta\left(\frac{1}{\xi^2}\right)\right]^2 + \left[D_0\frac{\Delta\left(\frac{1}{D_0}\right)}{\left(\frac{1}{D_0}\right)}\right]^2}$$

ΔD_0

$$= \sqrt{\left[\left(\frac{\left(\frac{1-\phi_A}{1+\phi_A}\right)^2}{\left(\left(\frac{1-\phi_A}{1+\phi_A}\right)^2\frac{1}{D} - \frac{1}{k\xi^2}\right)^2}\right)\Delta\left(\frac{1}{D}\right)\right]^2 + \left[\left(\frac{1}{k\left(\left(\frac{1-\phi_A}{1+\phi_A}\right)^2\frac{1}{D} - \frac{1}{k\xi^2}\right)^2}\right)\Delta\left(\frac{1}{\xi^2}\right)\right]^2 + \left[D_0\frac{\Delta\left(\frac{1}{D_0}\right)}{\left(\frac{1}{D_0}\right)}\right]^2}$$

$$\Delta D_0 = \sqrt{\left[D_0 \frac{\left(\frac{1-\phi_A}{1+\phi_A}\right)^2 \Delta\left(\frac{1}{D}\right)}{\left(\left(\frac{1-\phi_A}{1+\phi_A}\right)^2 \frac{1}{D} - \frac{1}{k\xi^2}\right)}\right]^2 + \left[D_0 \frac{\Delta\left(\frac{1}{\xi^2}\right)}{k\left(\left(\frac{1-\phi_A}{1+\phi_A}\right)^2 \frac{1}{D} - \frac{1}{k\xi^2}\right)}\right]^2 + \left[D_0 \frac{\Delta\left(\frac{1}{D_0}\right)}{\left(\frac{1}{D_0}\right)}\right]^2}$$

*Average values of $a\Delta(1/D)/(a*1/D-1/k\xi^2)$ and $\Delta(1/\xi^2)/(a*1/D-1/k\xi^2)$ were used and

$\Delta(1/D_0)/(1/D_0)$ comes from fitting of y-intercept ($1/D$ vs. $1/k\xi^2$) where $a = \left(\frac{1-\phi_A}{1+\phi_A}\right)^2$ is the

correction factor, and

$$\Delta k = \sqrt{\left[\left|\frac{\delta k}{\delta\left(\frac{1}{D}\right)}\right| \Delta\left(\frac{1}{D}\right)\right]^2 + \left[\left|\frac{\delta k}{\delta\left(\frac{1}{\xi^2}\right)}\right| \Delta\left(\frac{1}{\xi^2}\right)\right]^2 + \left[k \frac{\Delta\left(\frac{1}{k}\right)}{\left(\frac{1}{k}\right)}\right]^2}$$

$$\Delta k = \sqrt{\left[\left(\frac{\left(\frac{1-\phi_A}{1+\phi_A}\right)^2 \left(\frac{1}{\xi^2}\right)}{\left(\left(\frac{1-\phi_A}{1+\phi_A}\right)^2 \frac{1}{D} - \frac{1}{D_0}\right)^2}\right) \Delta\left(\frac{1}{D}\right)\right]^2 + \left[\frac{1}{\left(\left(\frac{1-\phi_A}{1+\phi_A}\right)^2 \frac{1}{D} - \frac{1}{D_0}\right)} \Delta\left(\frac{1}{\xi^2}\right)\right]^2 + \left[k \frac{\Delta\left(\frac{1}{k}\right)}{\left(\frac{1}{k}\right)}\right]^2}$$

$$\Delta k = \sqrt{\left[k \frac{\left(\frac{1-\phi_A}{1+\phi_A}\right)^2}{\left(\frac{1-\phi_A}{1+\phi_A}\right)^2 \frac{1}{D} - \frac{1}{D_0}} \Delta\left(\frac{1}{D}\right)\right]^2 + \left[k \frac{\Delta\left(\frac{1}{\xi^2}\right)}{\left(\frac{1}{\xi^2}\right)}\right]^2 + \left[k \frac{\Delta\left(\frac{1}{k}\right)}{\left(\frac{1}{k}\right)}\right]^2}$$

$$\Delta k = \sqrt{\left[k \frac{\left(\frac{1-\phi_A}{1+\phi_A}\right)^2 \Delta\left(\frac{1}{D}\right)}{\left(\left(\frac{1-\phi_A}{1+\phi_A}\right)^2 \frac{1}{D} - \frac{1}{D_0}\right)}\right]^2 + \left[k \frac{\Delta\left(\frac{1}{\xi^2}\right)}{\left(\frac{1}{\xi^2}\right)}\right]^2 + \left[k \frac{\Delta\left(\frac{1}{k}\right)}{\left(\frac{1}{k}\right)}\right]^2}$$

*Average values of $a\Delta(1/D)/(a*1/D-1/D_0)$ and $\Delta(1/\xi^2)/(1/\xi^2)$ were used and $\Delta(1/k)/(1/k)$

comes from fitting of slope ($1/D$ vs. $1/k\xi^2$) where a is the correction factor

Δln (k):

$$\Delta(\ln k) = \sqrt{\left[\left|\frac{\delta(\ln k)}{\delta k}\right|\Delta k\right]^2} = \left|\frac{\delta(\ln k)}{\delta k}\right|\Delta k = \left(\frac{1}{k}\right)\Delta k = \frac{\Delta k}{k}$$

ΔE_A (for Petit Model):

Activation energy is determined by fitting k vs T using

$$k = F_p e^{-E_A/RT}$$

Algebraically rearranging to solve for E_A gives

$$E_A = -RT\ \ln\left(\frac{k}{F_p}\right)$$

The uncertainty stems from k and T therefore

$$\Delta E_A = \sqrt{\left[\left|\frac{\delta E_A}{\delta T}\right|\Delta T\right]^2 + \left[\left|\frac{\delta E_A}{\delta k}\right|\Delta k\right]^2 + \left[E_A\frac{\Delta\left(\frac{E_A}{R}\right)}{\left(\frac{E_A}{R}\right)}\right]^2}$$

$$\Delta E_A = \sqrt{\left[\left(-R\ln\left(\frac{k}{F_p}\right)\right)\Delta T\right]^2 + \left[\left(\frac{RT}{k}\right)\Delta k\right]^2 + \left[E_A\frac{\Delta\left(\frac{E_A}{R}\right)}{\left(\frac{E_A}{R}\right)}\right]^2}$$

$$\Delta E_A = \sqrt{\left[E_A\frac{\Delta T}{T}\right]^2 + \left[E_A\frac{\Delta k}{k\ln\left(k/F_p\right)}\right]^2 + \left[E_A\frac{\Delta\left(\frac{E_A}{R}\right)}{\left(\frac{E_A}{R}\right)}\right]^2}$$

*Average values of $\Delta T/T$ and $\Delta k/|k\ln(k/F_p)|$ were used and $\Delta(E_A/R)/(E_A/R)$ comes from fitting of slope ($\ln k$ vs. $1/T$)

Δr_h:

Hydrodynamic radius is defined by

$$r_h = \frac{k_B T}{6\pi\mu D_0}$$

Uncertainty arises from T and D therefore

$$\Delta r_h = \sqrt{\left[\left|\frac{\delta r_h}{\delta T}\right|\Delta T\right]^2 + \left[\left|\frac{\delta r_h}{\delta D_0}\right|\Delta D_0\right]^2} = \sqrt{\left[\left|\frac{k_B}{6\pi\mu D_0}\right|\Delta T\right]^2 + \left[\left|\frac{-k_B T}{6\pi\mu D_0^2}\right|\Delta D_0\right]^2}$$

$$\Delta r_h = \sqrt{\left[r_h \frac{\Delta T}{T}\right]^2 + \left[r_h \frac{\Delta D_0}{D_0}\right]^2}$$

*Average values of $\Delta T/T$ were used.

$\Delta(1/\mu)$:

$$\Delta\left(\frac{1}{\mu}\right) = \sqrt{\left[\left|\frac{\delta\left(\frac{1}{\mu}\right)}{\delta\mu}\right|\Delta\mu\right]^2} = \left|\frac{\delta\left(\frac{1}{\mu}\right)}{\delta\mu}\right|\Delta\mu = \left(\frac{1}{\mu^2}\right)\Delta\mu = \left(\frac{1}{\mu}\right)\frac{\Delta\mu}{\mu}$$